[Type here]


Politecnico di Torino

# Politecnico di Torino

Corso di Laurea Magistrale in Ingegneria Energetica e Nucleare

## *Techno-economic analysis of a CCU process based on CO2 capture by PSA and its conversion to synthetic methane using renewable hydrogen*

**Supervisor:** Massimo Santarelli

**Co-supervisors:** Salvatore Francesco Cannone, Domenico Ferrero

**Candidate:** Gianmarco Catapano

# CONTENTS

CHAPTER 1: INTRODUCTION ..... 6
1.1 Energy transition ..... 7
1.2 Carbon capture and utilization (CCU) ..... 9
1.3 Power-to-X ..... 11
1.4 Biogas ..... 12
1.5 Objective of the work ..... 16
CHAPTER 2: PRESSURE SWING ADSORPTION ..... 17
2.1 Skarstrom cycle ..... 18
2.2 Adsorption process ..... 19
2.2.1 Gas Adsorption equilibrium ..... 20
2.2.2 Mass, energy and momentum balance equations ..... 21
2.2.3 Adsorption kinetics ..... 23
2.3 Adsorbent materials ..... 24
2.4 TSA and VPSA systems ..... 25
2.5 Performance Metrics ..... 26
CHAPTER 3: WATER ELECTROLYSIS and METHANATION PROCESS ..... 27
3.1 Electrolyzer technology ..... 28
3.1.1 Akaline water electrolysis (AWE) ..... 29
3.1.2 Proton Exchange Membrane Water Electrolysis (PEMWE) ..... 30
3.1.3 Solid Oxide Electrolysis (SOEC) ..... 31
3.2 Fundamentals on electrolysis ..... 32
3.3 Thermodynamic model ..... 33
3.4 Electrochemical model ..... 34
3.4.1 Polarization curve ..... 35
3.4.2 Faraday efficiency ..... 37
3.4.3 Gas purity model ..... 38
3.5 Principles of methanation ..... 40
**3.5.1** ***TREMPTM*** process description ..... 40
CHAPTER 4: MODEL AND RESULTS ..... 43
4.1 Pressure Swing Adsorption configuration ..... 44
4.1.1 Input specifications ..... 45

4.1.2 Output simulation ..... 48
4.2 Electrolyzer Model ..... 54
4.2.1 Electrolyzer Aspen model ..... 59
4.2.2 Methanation section ..... 60
4.2.3 Natural gas correction ..... 60
4.3 Plant efficiency ..... 62
4.4 Economic analysis ..... 64
4.4.1 Capex plant ..... 65
4.4.2 Opex plant ..... 65
4.4.3 Results ..... 66
4.4.4 Sensitivity analysis ..... 68
CONCLUSIONS ..... 70
References ..... 72

# ABSTRACT

Nowadays climate change due by global warming has a significant role for the human civilization. The major greenhouse gas (GHG) is the carbon dioxide, $CO_2$, and its rising concentration in the atmosphere leads to an increase of the surface temperature in the Earth. Over the last decade, considerable research has been conducted to explore the utilization of $CO_2$ together with $H_2$ in order to produce synthetic natural gas ($CH_4$) and water ($H_2O$) but the process is still not feasible for large-scale applications.

The use of renewable energy sources (RES) is an alternative way to produce energy than the fossil fuels with the aim of reducing carbon emissions. They include bioenergy, hydropower, geothermal energy, solar energy and wind energy and are considered clean sources of energy and the optimal use of these sources decrease the environmental impacts and are sustainable based on the future economic and social needs.

This work investigates the feasibility of integrating a carbon capture process as the Pressure Swing Adsorption (PSA) with an alkaline electrolyser in order to produce synthetic natural gas(CH4) via $CO_2$ hydrogenation with the possibility to inject the natural gas in the distribution grid with a Power-to-X path.

The PSA system was developed in MATLAB, while the alkaline electrolyzer and the methanation reactor were modelled using Aspen Plus. The PSA model consist of a code that simulates a 2 bed capture system with solid sorbents for the biogas upgrading and obtaining a product stream with a high amount of carbon dioxide ($CO_2$). Subsequently the captured $CO_2$ stream is mixed with the hydrogen produced from the electrolyzer and sent to a reactor for methanation process.

The study evaluated the performance metric of PSA system and the AWE performance focusing on their operational efficiency. In addition the overall system efficiency was analysed, highlighting its potential as sustainable solution for decarbonization process.

# CHAPTER 1: INTRODUCTION

The growing global demand for energy, combined with a strong reliance on fossil fuels, has significantly increased the concentration of greenhouse gases in the atmosphere, reaching critical levels. Of these gases, carbon dioxide ($CO_2$) is the primary driver of global warming, accounting for roughly 76% of total greenhouse gas emissions, followed by methane ($CH_4$) at 16%, nitrous oxide ($N_2O$) at 6%, and other gases at approximately 2% [1]. Among these gases, carbon dioxide is considered the primary contributor to global warming due to its high concentration. To mitigate the harmful effects of climate change and reduce emissions, various technologies have been developed in recent decades to capture and recover carbon dioxide ($CO_2$) in different scenarios.

The use of renewable energy sources (RES) provides an alternative to fossil fuels, aiming to reduce society's dependency on carbon-based energy. However, many renewables, like wind and solar, generate power intermittently and often produced far from where it is needed. As a result, there is considerable interest in developing methods for the long-range transport and storage of renewable energy. Additionally, renewable energy sources can be used to produce hydrogen through water electrolysis, while carbon dioxide can be combined with hydrogen and catalytically converted into synthetic natural gas (SNG).

The combustion of natural gas produces the lowest ratio of emitted CO2 per unit of thermal energy produced. Natural gas is flexible because is largely used in transportation, electricity production and civil heating sectors. The use of electrolyzers for energy conversion has generated a great deal of interest in recent years. Alkaline electrolyzers are able to convert electrical energy into chemical energy via water electrolysis.

The aim of this work is to simulate a plant for synthetic natural gas production. The final product can be directly injected into the national distribution gas grid. The plant consists of mainly different parts: the carbon capture with Pressure Swing Adsorption (PSA) simultaneously with water electrolysis section followed by a catalytic process called methanation or hydrogenation of CO2 and a cleaning with correction section in order to meet the grid parameters for SNG.

The work consists of a first theoretical section where the main concepts of adsorption process, technology and electrolyzers are treated, focusing on both the thermodynamics features of the systems and the state of the art of the technologies. Then, attention is paid on methanation process coupled with AWE. The main goal of this analysis is the calculation of overall plant efficiency as the ratio of SNG chemical energy and electricity input required.

In the end, an economic analysis is carried out to assess the feasibility of the plant and to calculate the LCOP in order to compare it with the cost of natural gas currently market in the residential and industrial sector.

## 1.1 Energy transition

Humanity currently faces one of the most critical challenges when global temperatures rise progressively. Multiple factors create this issue though carbon dioxide emissions remain the principal contributor. In 2021, carbon dioxide emissions from energy production totalled 36.3 gigatonnes, predominantly resulting from our reliance on fossil fuels [2]. The issue of these emissions is considered to be a critical challenge which is hard to solve since many industries are still heavily reliant on fossil energy sources. The current reliance on fossil fuel combustion for energy uses makes it necessary to create new low-carbon technologies aimed at emission reduction. Some sectors prove difficult to decarbonize through simple electrification because renewable energy technologies face obstacles through their developments.

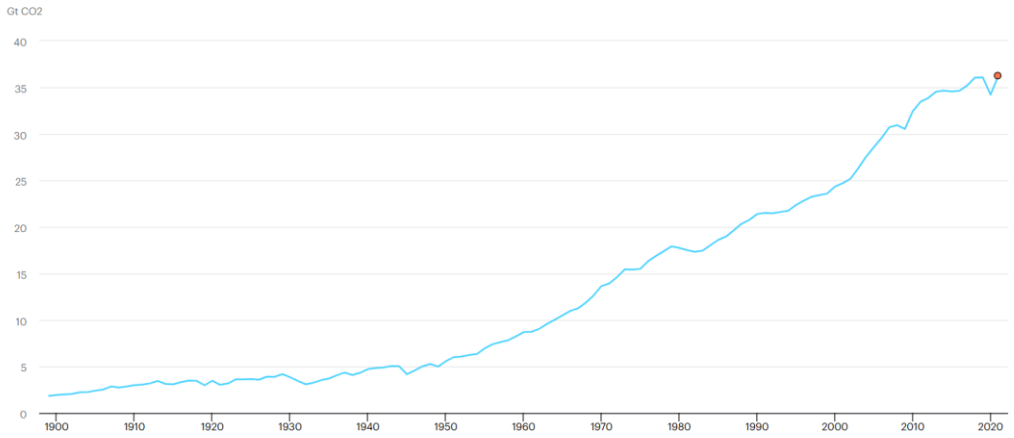


*Figure 1.1 - $CO_2$ emissions scenario*

The power and heavy industry sectors are expected to produce the largest cumulative emissions from existing infrastructure, because they are the largest emitters now and their assets last a long time. Additionally, at a current global energy scenario, coal is the biggest contributor to global energy related $CO_2$ emissions since it is the most carbon intensive fossil fuel, as we can see from fig 1.2, used from energy infrastructure. [3].

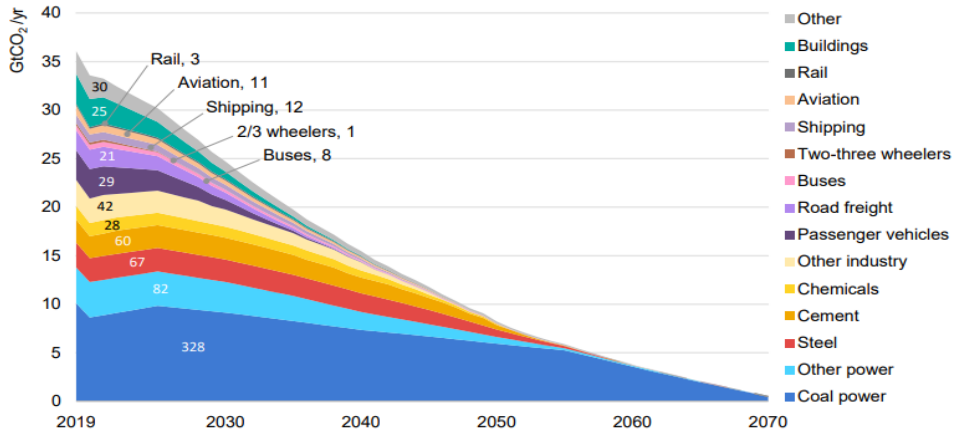


*Figure 1.2 – Global $CO_2$ emissions by sub-sector*

The energy sector requires a radical technological transformation to achieve net-zero $CO_2$ emissions which makes this both an urgent and essential challenge. The central nature of energy efficiency and renewable energy does not exclude additional technologies such as end-use sector electrification through advanced batteries, carbon capture, utilization and storage (CCUS), hydrogen and hydrogen-related fuels and bioenergy for achieving net-zero emissions. The worsening of global warming demands that recent research focus on these technologies that help decrease greenhouse gas emissions toward reaching net-zero emissions.

As has been mentioned above, the strategies that have been proposed include those that are likely to put the emission levels on a path towards net zero. Suggesting that technologies such as CCS (Carbon Capture and Storage) or CCU (Carbon Capture and Utilization) should be developed especially in the initial stage of the ecological transition when fossil fuels will remain the dominant source of energy. Research shows that CCS can help to reduce emissions by up to 19% by 2050 by trapping $CO_2$ from industrial gases. The main benefit of these technologies is that they can be easily integrated into current production facilities, thus cutting down on carbon dioxide emissions. However, the expenses connected with the capture, transportation, and storage of the carbon dioxide have to be considered. Instead, the pollutant can be given a positive value through treatment, rather than being considered as waste (a compound of negative value). The technologies applied in this regard are known as CCU and they are used to capture the $CO_2$ and convert it into a valuable product. Thus, the capture and conversion method not only decreases the emissions but also produces the chemical energy. The $CO_2$ captured from power plants is employed as a reagent to produce primarily two categories of products: Fuels or chemical intermediates that can be used as the feedstock in the chemical industry. [4].

An important role in this scenario includes the $CO_2$ to methane conversion through green hydrogen which operates as a light fuel while producing low $CO_2$ emissions per energy unit. The conversion of $CO_2$ to methane occurs through several methods including photocatalysis and electrochemical reduction as well as biological conversion with enzymes and thermal methanation. Power-to-Gas systems have been thoroughly researched as storage solutions for surplus renewable electricity which transforms into methane through various studies. The creation of methane enables subsequent storage and distribution through current pipeline networks thus reducing required capital investments. The strategy provides substantial flexibility and has the ability to help stabilize electrical grids that contain high amounts of renewable energy while driving long-term decarbonization. Green hydrogen has gained increasing attention in recent years because it represents an energy carrier which derives its energy from renewable sources and will play a key role in upcoming energy transitions. The energy-rich fuel hydrogen operates as a clean power source because it emits no polluting substances during operation. The intermittent nature of most renewable sources makes electrical energy storage technologies expensive, so hydrogen production from electricity represents a viable alternative. The method keeps excess electrical power from going unused because it converts this energy into chemical form. [5].

## 1.2 Carbon capture and utilization (CCU)

The concept of using carbon capture and utilization (CCU) has emerged as a recent technological solution to address both greenhouse gas emissions as well as increasing global energy needs. To fight climate change caused by $CO_2$ emissions, initiatives have started $CO_2$ capture and sequestration from major point sources, power plants, but using $CO_2$ as an input to create valuable chemicals, materials and transport fuels holds more promise as a lasting solution.

Carbon dioxide can be captured from $CO_2$ containing gases by using technologies, which are commercially available and established in chemical processing. The main challenges are the large flue gas flows, the chemical composition of flue gases, a high degree of $CO_2$ purity and the $CO_2$ capture rate. Worldwide, studies are focusing at present on identifying energy and cost-efficient capture solutions. The purity of the $CO_2$ stream after separation is the most influencing factor for how much energy is needed for the capture of $CO_2$ but also is a significant aspect for the transport, storage and exploitation of the carbon dioxide stream. With increasing requirements regarding the purity of the $CO_2$, its capture is more expensive and requires more energy. There are different commercial technologies to capture carbon dioxide from gases and the most discussed processes are [6]:

- **Post-combustion**: $CO_2$-capture from the flue gas stream after combustion;
- **Oxy-fuel**: use of nearly pure oxygen for fuel combustion instead of air which increases the $CO_2$- concentration of the flue gas;
- **Pre-combustion**: $CO_2$-capture from the reformed synthesis gas of an upstream gasification unit.

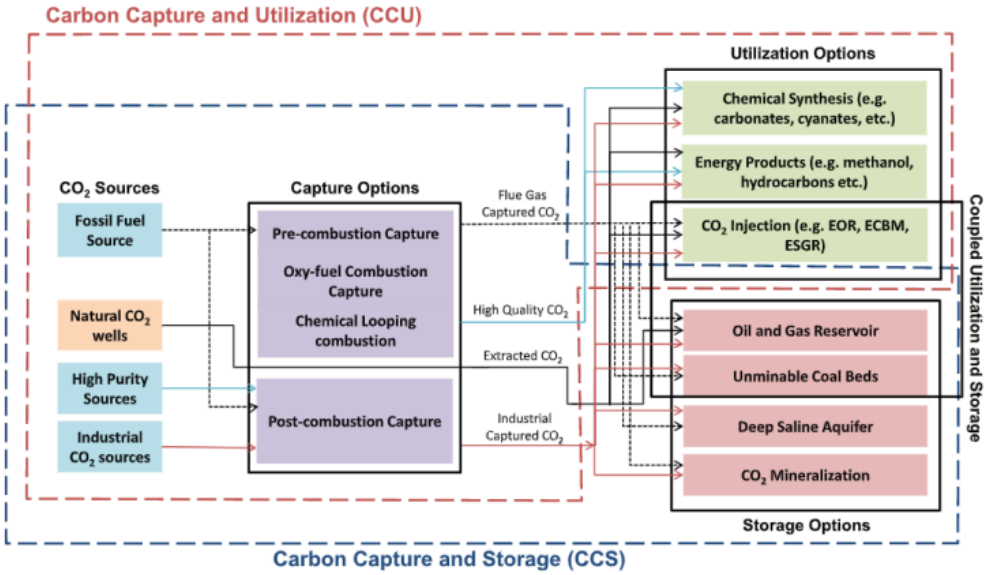


*Figure 1.3 - Recycle and Utilization of $CO_2$*

Over the years, a variety of $CO_2$ capture techniques have been developed, such as absorption, adsorption, membranes, and other innovative methodologies. Among these, absorption predominantly employing chemical solvents ,such as amines, stands as the most advanced and widely adopted technique for large scale $CO_2$ capture.

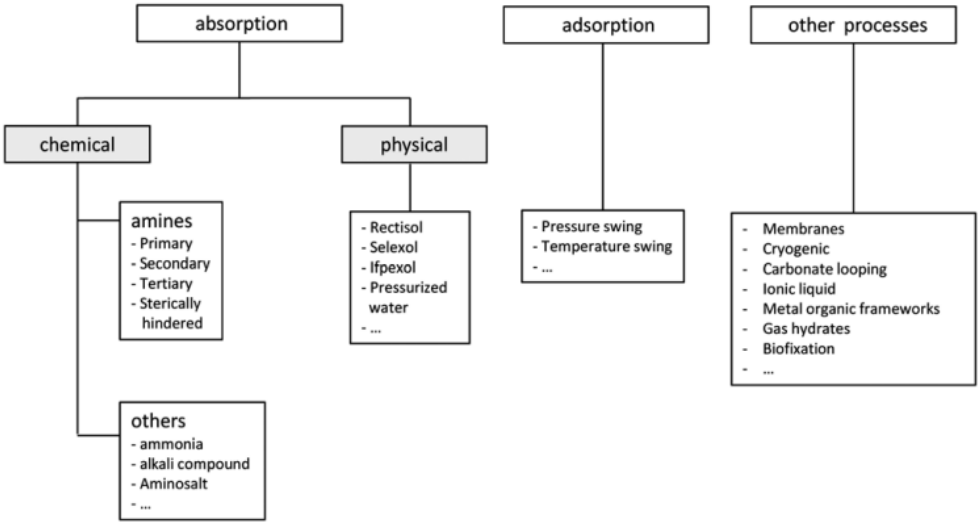


*Figure 1.4 – Principles for Carbon Capture*

In close relation to the thesis work, another approach to carbon capture (CC) is gas-solid adsorption, where $CO_2$ is captured using solid adsorbents, typically in a fixed bed configuration of particles such as activated carbons and zeolites that have been pioneering the development of solid adsorbents for $CO_2$ capture. $CO_2$ adsorption requires a regeneration process. Two beds are used one for $CO_2$ adsorption and the other for regeneration and removal, a process done through either pressure swing adsorption (PSA) or temperature swing adsorption (TSA). [7].

## 1.3 Power-to-X

The integration of several energy systems is expected to provide a more efficient use of renewable energy sources in current systems and support the significant decarbonization targets set forth.

Power-to-X (P2X) refers to different methods enabling electric power conversion together with storage and subsequent conversion into several energy products [8]. These technologies are especially useful in energy systems that have a high penetration of renewable energy or those that have set aggressive decarbonization goals. The term "X" refers to the specific energy form into which electricity is transformed, which can include gases, liquids, or heat. This can include power-to-ammonia, power-to-hydrogen, power-to-gas, power-to-liquid, power-to-power, and others.

The generation of electricity from wind and solar sources is highly dependent on weather factors and time of year, thus requiring large-scale energy storage systems to address the variability in power production. One way of dealing with surplus electricity is to use one of the Power-to-X pathways to convert the energy.

Another important objective of the Power-to-X concept is to utilize the surplus renewable energy to produce hydrogen and oxygen through the water electrolysis process. In electrolyzers, direct current flow is used to produce hydrogen, which can then be converted into methane through the methanation process. Alternatively, hydrogen can be produced by reacting with carbon dioxide to give methanol. Methane and methanol can be stored and then used to produce electricity, with storage duration ranging from hours to months.

The Power to Gas (PtG) process chain is a crucial component of the future energy system in which renewable electrical energy can be stored in the form of methane through electrolysis followed by methanation [9]. This concept starts by extracting $CO_2$ from exhaust gases, through Pressure Swing Adsorption (PSA) process and on the other side, $H_2$ is produced from water electrolysis using the electricity supplied by renewable energy systems. Finally the production of Methane ($CH_4$) can be achieved by combination of the captured $CO_2$ and the extracted $H_2$ via a reactor known as a reactor of Sabatier, this operation is called methanation.

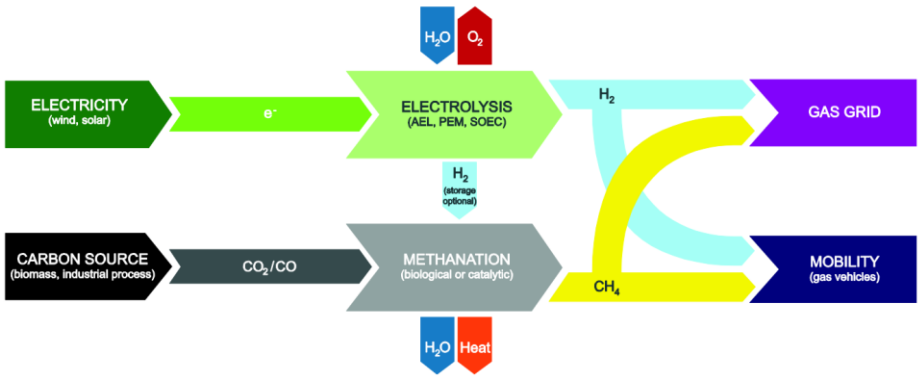


*Figure 1.4 - Power-to-Gas process chain*

## 1.4 Biogas

The emerging market for renewable energy sees biogas playing a key role. Bioenergy looks set to provide a quarter of the EU-27's renewable energy target for 2020 and biogas will make up at least 25% of this. More than double the global capacity for power generation from commercial biogas facilities will be reached by the end of this decade: 14.5 gigawatts (GW) in 2012 to 29.5 GW in 2022. [10]. Due to research and innovation there has been an increase in efficiency in the biogas sector and it is also developing and growing. Germany has the highest practice of biogas in Europe, but Italy is second in Europe, as we can see in fig.1.6 [11].

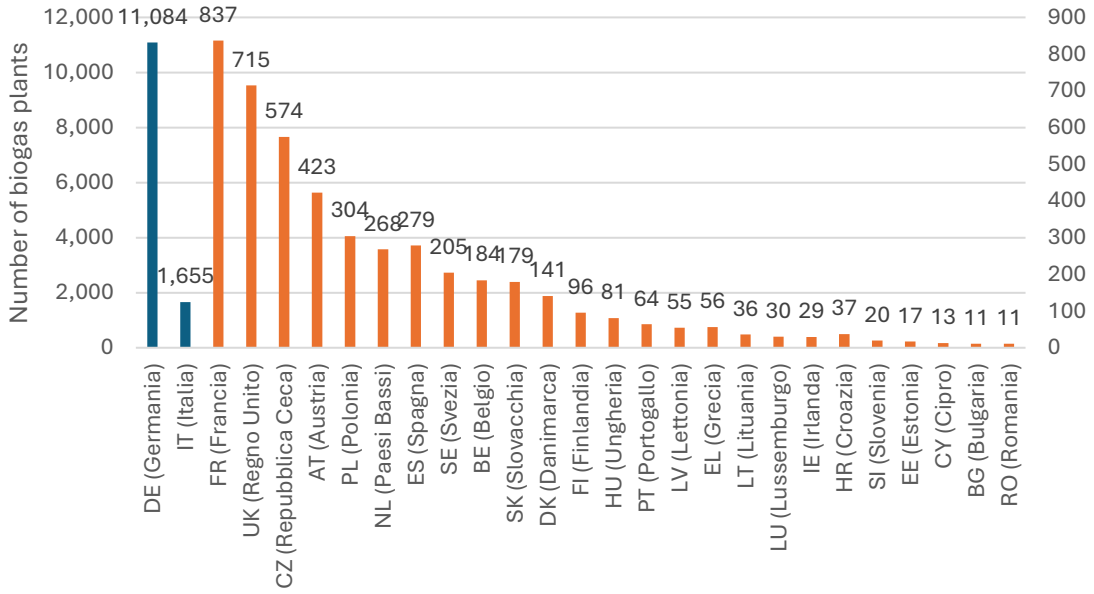


*Figure 1.6 – Total number of biogas plants (2018)*

The fig.1.7 shows the development over the last years of the biogas plants for electricity generation and the installed capacity. The number of plants and the overall installed capacity have significantly increased, especially in the period between 2008 and 2013, as a result of incentives and improvement in the technology of anaerobic digestion. Most of the contribution is made by Northern Italy (83.4% of the national total) as the region is highly populated with cattle farming and swine breeding. This high level of livestock farming provides a relatively constant supply of manure, which, together with agricultural residues and energy crops, is a crucial raw material for biogas production. Biogas utilization in electricity production is one of the most important ways of reducing greenhouse gas emissions and can contribute to the process of decarbonizing the energy sector. In 2019, the first region in terms of biogas production is Lombardy, with 34.6% [12].

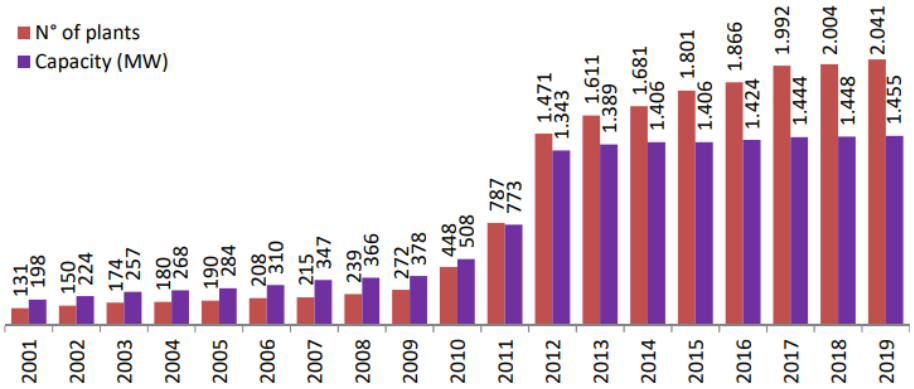


*Figure 1.7 – Evolution of biogas plants in Italy*

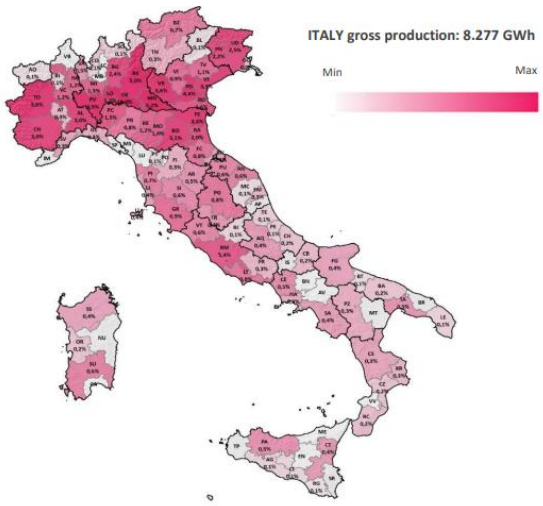


*Figure 1.8 – Distribution of biogas plants for electricity production in Italy (2019)*

Biogas is produced by microbial anaerobic digestion (AD) of the organic mass through four processes: hydrolysis, acidogenesis, acetogenesis, and methanogenesis by which microorganisms break down biodegradable material in the absence of oxygen. It is composed mainly of methane ($CH_4$) and carbon dioxide ($CO_2$), in different concentration depending on the source production, and other trace gas [13]. There are a wide range of feedstocks for biogas production using AD process in Europe:

- **Agriculture**: largest contributor to biogas production are livestock manure, crop residues, and energy crops such as maize silage. Agricultural waste is a steady and renewable source of biomass, which makes it a major component in anaerobic digestion processes.
- **Sewage**: wastewater treatment plants contribute substantially to the organic waste that serves as feedstock for biogas production.
- **Landfill**: another form of biogas is produced from organic matter decomposition in landfill sites. This approach helps to capture methane emissions that would otherwise make their way into the atmosphere and this has the advantage of reducing greenhouse gas emissions.

- **Other**: this category encompasses a variety of organic waste sources including food waste, industrial byproducts and organic fractions of municipal solid waste, which can be used in biogas production.

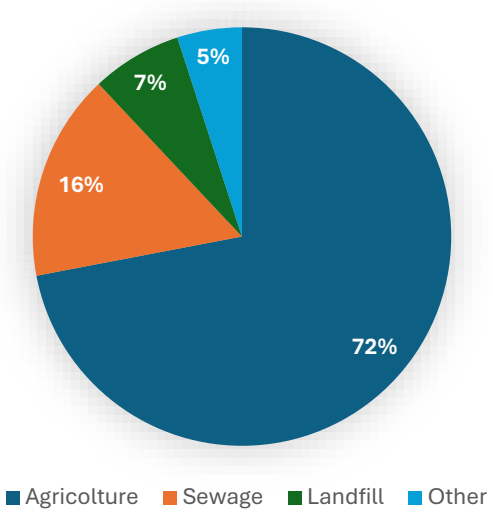


*Figure 1.9 Typical feedstocks in biogas plant*

Upgrading biogas to biomethane is one of the technologies that attract great interest in the bioenergy industry. The raw biogas produced from organic biomass wastes through the AD processes consists majorly of biomethane ($CH_4$) and carbon dioxide ($CO_2$). Aside from the $CH_4$ and $CO_2$, the raw biogas also contains some small or minor amounts of hydrogen sulphide ($H_2S$), ammonia ($NH_3$), water vapour ($H_2O$), nitrogen ($N_2$), oxygen ($O_2$), carbon monoxide (CO), hydrogen ($H_2$), siloxanes and hydrocarbons which are regarded as impurities or pollutants. When the biogas is purified or cleaned and upgraded to required specifications that are similar to natural gas, the final gas product is called biomethane. The largest producer of biomethane in Europe is Germany, with 242 biomethane plants in 2020 [14].

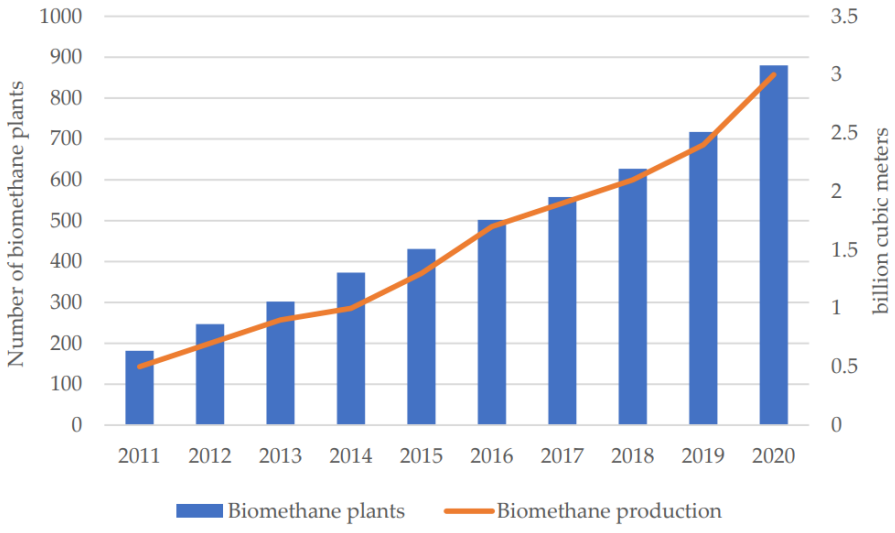


*Figure 1.10 – Number of biomethane plants and biomethane production in Europe (2021)*

There are different technologies of upgrading with different performance in terms of purity of methane, losses and efficiency [10]:

- Pressurized water scrubbing (PWS): is the most used and consolidated technology, it can achieve a purity of 80-99% with low losses 3-5%, in some case lower than 2%. The energy consumption, only electric power, is mainly used to compress raw gas and processing water.
- Physical absorption (PA): is similar to PWS but instead of water it is used an organic solvent to have a higher solubility of the CO2, the system needs thermal power to regenerate the solvent.
- Chemical absorption (CA): the solvent, usually amines, react selectively with carbon dioxide to remove it from the biogas. The technology can reach a high purity of methane (99%) and CO2 but a large amount of thermal energy is needed to regenerate solvent.
- Cryogenic separation (CS): the methane and carbon dioxide are separated by condensation and distillation. This technology is still under development and has a high energy demand and it is economical expensive, but it allows to obtain a high concentration of methane in the product, and also a high concentration of carbon dioxide in byproduct.
- Pressure swing adsorption (PSA): the process is based on the selective adsorption on the solid surface of the molecule based on their size. The concentration of CH4 is between 96% and 98% but higher is the purity request higher are the losses of methane.
- Membrane separation (MS): is based on the selective permeability of membrane which can be crossed by CO2 and not by CH4. MS is considered cheap, simple and efficiency but is not possible to achieve high methane concentration without many stages.

One of the most widely used technologies today Europe is the membrane separation, due to its low operating costs and no solvents in the process. Figure 1.11 shows the situation in Europe in terms of upgrading technologies [14].

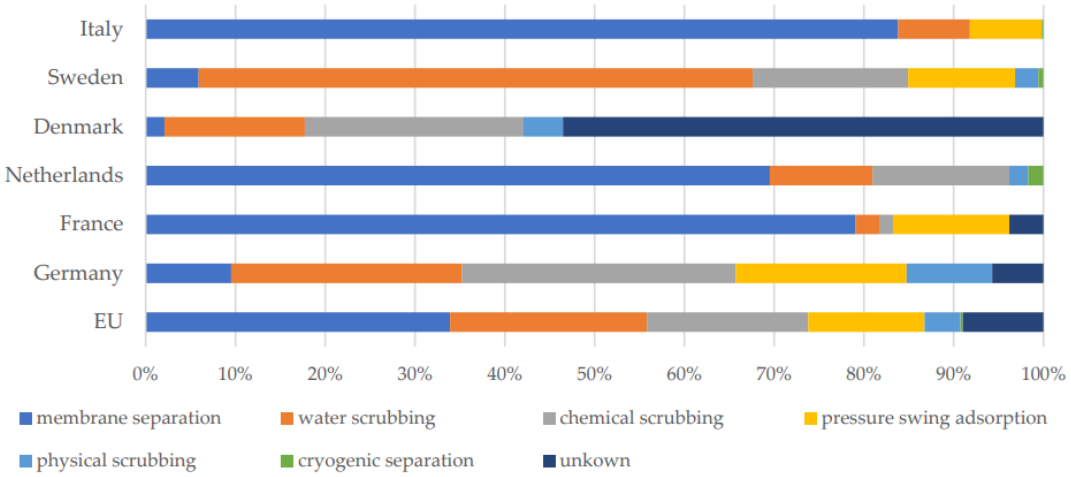


*Figure 1.11 – Biomethane upgrading methods in Europe (2020)*

## 1.5 Objective of the work

The objective of the thesis is to simulate a plant for synthetic natural gas production. The final product can be directly injected into the national distribution gas grid. Firstly, a development and a simulation of a Pressure Swing Adsorption (PSA) system is performed on MATLAB, for biogas upgrading in order to collect the output $CO_2$-rich stream. In addition, an alkaline electrolyzer and the methanation reactors are designed on Aspen Plus. The performance of the two systems is measured and compared to find the best operational conditions, evaluating the overall efficiency demonstrating the potential of the whole system as a sustainable solution for the decarbonization process. In the end, an economic analysis is done to assess the feasibility of the plant and compare costs with those of natural gas currently marketed in the residential and industrial.

The work is divided in four chapters:

**Chapter 1** A review of the energy scenario and the technological pathways for the transition toward a low carbon energy system, such as Carbon Capture and Utilization (CCU), Power to Gas and biogas upgrading.

**Chapter 2** The description of the principles of Pressure Swing Adsorption (PSA) system exploring the main design features, adsorbent materials, alternative swing processes, and key performance metrics for evaluating system effectiveness.

**Chapter 3** A brief overview of technologies involved (i.e. alkaline water electrolysis and methanation) is presented. Then the description of the mathematical model of an alkaline electrolyzer is presented and created on Aspen Plus.

**Chapter 4** Systems analyses are presented. At first sensitivity analyses to evaluate the behaviour of PSA and electrolysis by varying some operational parameters is realized. Then an evaluation of the whole system is made. At the end, the economic analysis has the aim of an estimation of SNG production cost.

# CHAPTER 2: PRESSURE SWING ADSORPTION

Gas separation on an industrial scale is vital to many processes, employing various techniques including absorption, cryogenic distillation, membrane separation, and adsorption. Among these methodologies, adsorption has proven to be a particularly viable option owing to its relatively low operational costs and high energy efficiency. This technique utilizes highly porous materials, such as activated carbons, which are either commercially available or under continual development through advancements in material science and engineering.

A practical solution for integrating carbon capture into existing energy frameworks is Carbon Capture. Within the paradigm of $CO_2$ capture via adsorption, Pressure Swing Adsorption (PSA) stands out as the most widely utilized technology on an industrial scale. PSA operates as a cyclic adsorption process designed for the continuous separation of gas streams by leveraging periodic pressure variations to enhance the removal of contaminants. This technology is particularly adept at separating $CO_2$ from flue gases that contain approximately 5–15% $CO_2$ [1].

The selection of adsorbent material is a critical determinant of the overall efficiency of a PSA system. The performance of the unit is contingent on key properties of the adsorbent, as well as various process parameters including cycle configuration, the number of columns, cycle duration, bed length, and the composition of the inlet gas mixture. A standard PSA cycle typically encompasses four essential operational steps: pressurization, feed, blowdown, and purge. The design and optimization of PSA systems involve complex challenges that necessitate a thorough understanding of process dynamics to attain the desired separation efficiency.

Capturing biogas not only mitigates its release into the atmosphere but also facilitates its use as a renewable and sustainable energy source or fuel. However, due to the fact that biogas generally contains around 40–70% methane, its immediate application is typically confined to power or heat generation in proximity to the site of production. For wider applications, particularly as a transportation fuel or for injection into the existing natural gas pipeline network, biogas necessitates an upgrading process [15]. The predominant contaminant in biogas is carbon dioxide ($CO_2$), represents roughly 30–60% of its composition. Consequently, upgrading biogas to biomethane entails an efficient bulk separation process to ensure that the end product adheres to the pipeline-quality standards set by each country for natural gas distribution. Various technologies have been developed for this purpose, among which adsorption-based processes, particularly Pressure Swing Adsorption (PSA), have shown considerable promise for the purification of biomethane.

For biogas upgrading in order to collect CO2, this thesis investigates a PSA system that provides a comprehensive framework for the dynamic modelling and simulation of PSA processes, implemented within an open-source simulator known as toPSAil [16].

## 2.1 Skarstrom cycle

Pressure swing adsorption, its concept was first introduced by Skarstrom in the 1960s when he received a patent for a two-bed air separation system [17]. Standard PSA cycles encompass operational and regeneration phases. A Skarstrom PSA cycle is represented in the figure below for a single adsorber utilizing re-pressurization with product gas. The feed is assumed to be a binary gas mixture, with the light key component (the species that is less preferentially adsorbed) and the heavy key collected as the raffinate and the extract products . Initially, the adsorber operates at low pressure, with a gas-phase composition closely matching that of the desired product, while the adsorbed phase is near equilibrium with this gas.

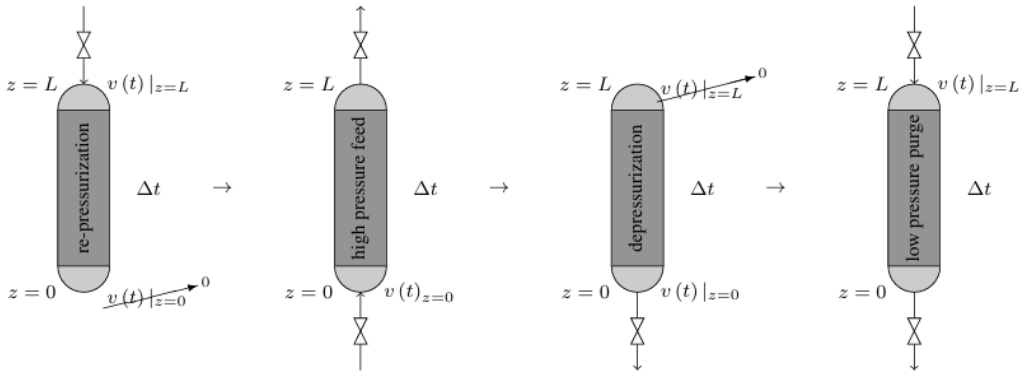


*Figure 2.1 - Skarstrom cycle for a single bed*

The process is composed of four essential steps:

1. **Re-pressurization:** the column is taken up to the target operating pressure by adding previously collected raffinate product gas from the top of the column.

2. **High-Pressure Feed:** the raffinate product is collected from the top while feed gas is introduced at elevated pressure from the lower column section. This phase continues until the adsorbent gets saturated with the heavy key component, thereby reducing product purity below a specified threshold. This breakthrough is the signal for the start of the regeneration phase.

3. **Depressurization:** vented at the bottom, the pressure is returned to its initial low state. This pressure reduction helps in the desorption of the species adsorbed.

4. **Low-Pressure Purge:** At the top of the column, raffinate product gas is introduced to clear residual gas from the void space and thus restore the system to its original condition.

As pressure procedures, re-pressurization and depressurization operate with column sealing at one end while pressure at the other end is manipulated using a valve. The column operates at constant pressure throughout high-pressure feed and low-pressure purge steps. Most of these operations keep constant and stepwise volumetric flow rates that are controlled by mass flow controllers.

During the feed step, back pressure control regulates the outlet volumetric flow rate to preserve column pressure as designated. During the purge step, the outlet valve opens fully to atmosphere so gas exits at ambient pressure. Practical implementation fails to achieve ideal pressure constancy since column length produces varying pressure across its span. Product tank operation at slightly lower feed gas pressure produces a pressure deficit at re-pressurization step end. A small pressure spike occurs briefly when feed step activation begins.

## 2.2 Adsorption process

Adsorption is a complex process where molecules move from the bulk fluid phase to bind with the surface of a solid adsorbent [18]. This mechanism is very important for gas separation and purification processes. For the modelling purposes the adsorption can be considered as taking place in three consecutive phases. The procedure encompasses the following key stages:

- Diffusion of the adsorbate from the bulk fluid phase into the pores of the solid adsorbent
- The molecule is adsorbed into the porous medium and localised within the pore space, held by intermolecular forces including van der Waals forces or chemical bonding that hold the adsorbate to the solid.

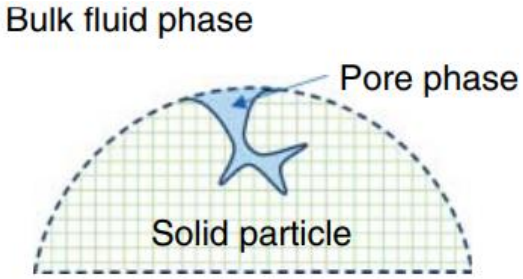


*Figure 2.2 - Pashes in the adsorption process*

The principal force responsible for the adsorption process is the concentration difference between the bulk fluid and the pore space. This phenomenon is based on a basic concept: if a particular chemical species is highly concentrated in the bulk phase but low in the pore phase, then diffusion will naturally occur to equalize the concentrations.

Further, advanced adsorption models also take into consideration other factors like the presence of a laminar boundary layer around the adsorbent particle which affects the rate of mass transfer. Moreover, these models may include internal concentration gradients within the porous medium that influence the overall adsorption efficiency. In some cases, advanced simulations can also explain the movement and arrangement of the adsorbed molecules on the surface of the solid, especially when competitive adsorption or surface diffusion effects are important. However, for most practical purposes in adsorption based unit operations, such detailed modelling is not required as bulk diffusion and surface adsorption give a sufficiently good idea of the system. In industrial terms, adsorption is divided into physical adsorption, or physisorption, and chemical adsorption, or chemisorption.

Physisorption is based on the weak van der Waals forces and is generally reversible and thus more appropriate for processes such as Pressure Swing Adsorption (PSA) [19].

The efficiency of adsorption depends on the characteristics of the adsorbent such as surface area and porosity, the conditions of pressure and temperature of the system and the adsorbate-adsorbent interaction force. These parameters can be optimized to make adsorption technologies work effectively in carbon capture, biogas upgrading, and industrial gas purification.

### 2.2.1 Gas Adsorption equilibrium

Under given conditions of temperature and pressure, an equilibrium is established between the amount of species adsorbed by an adsorbent and the fluid phase concentration of the adsorbate when they come into contact with each other. The adsorption isotherms are of great importance in determining the adsorption capacity, improving the adsorption processes and designing various industrial separation systems.

Multiple mathematical models known as the Freundlich Langmuir Redlich–Peterson and Sips isotherms have been developed to model single-component adsorption equilibrium. Each model is predicated on different assumptions regarding the surface properties of the adsorbent, the adsorption energy distribution, and the intermolecular forces. Because there are numerous adsorption isotherm models available, the choice of the best one depends on the characteristics of the adsorbent material and adsorption process. Due to the flexibility of the isotherms to fit complex adsorption data, the focus was made on a certain model: the Sips (Langmuir-Freundlich) isotherm.

The Langmuir isotherm that is based on the assumption that adsorption takes place at homogeneous active sites, where each site can hold only one molecule (monolayer adsorption). On the other hand the Freundlich isotherm assumes that adsorption occurs on a heterogenous surface describing porous and irregular surfaces [20]. The Sips is an hybrid model combining features of both the Langmuir and Freundlich equation and describes systems where the adsorption sites are homogeneous or heterogeneous with the following equation [19]:

$$q_i = \frac{a_i \; c_i^n}{1 + \sum_{j=1}^{NC} b_j \; c_j^n} \tag{1}$$

where:

- $q_i$ : amount of adsorbate adsorbed per unit mass of adsorbent for component iii ;
- $a_i$: maximum adsorption capacity for the component $i$ (related to Langmuir adsorption);
- $c_i$: equilibrium concentration of the adsorbate in solution;
- $n$ : heterogeneity factor (if $n$ =1, the model reduces to the Langmuir isotherm; if $n$ < 1, it indicates surface heterogeneity);

- $b_j$: affinity constant of the component $j$ (related to adsorption strength);
- $NC$: number of components in a multi-component adsorption system;
- $\sum_{j=1}^{NC} b_j \ c_j^n$: represents the competitive adsorption effects in a multi-component system.

### 2.2.2 Mass, energy and momentum balance equations

The performance of a Pressure Swing Adsorption (PSA) system can be attributed to mass transfer, heat transfer and fluid dynamics in the adsorption columns. These processes are modelled by three fundamental balance equations: the mass balance governs the transport and adsorption of gas species, while the energy balance takes into account the heat effects resulting from adsorption and desorption, the momentum balance equation describes the pressure drop along the bed. Each of these equations is solved as a partial differential equation (PDE) and solved together with other equations to get the dynamic behaviour of the PSA system.

The mass balance equation for a packed bed equation specifically describes how concentration of each gas component changes along the fixed bed including terms such as accumulation term, convection transport, uptake of the adsorbate and axial dispersion [21]. It is given by:

$$\frac{\partial c_i}{\partial t} + \frac{\partial}{\partial z}[u_{in} c_i] + \frac{(1-\varepsilon_b)}{\varepsilon} \rho_p \frac{\partial q_i}{\partial t} - Đ \frac{\partial c_i^{\,2}}{\partial z^2} = 0 \qquad (2)$$

Where $c_i$ is the concentration of a component, $u_{in}$ is the axial velocity of the fluid along the bed, $\varepsilon_b$ is the bed porosity, $q_i$ is the adsorbed phase concentration, $\rho_p$ is the adsorbent particle density and Đ is the axial dispersion coefficient which includes contributions from both molecular diffusion and hydrodynamic dispersion.

To take into account the energy balance, three different balances were employed: one for the bulk gas phase, the adsorbed phase plus the solid adsorbent phase, and the adsorber wall [19]. The energy balance for the gas phase is expressed by:

$$-k\varepsilon_b \frac{\partial T^2}{\partial z^2} + \rho_g C_{v,g} \varepsilon_b u_{in} \frac{\partial T}{\partial z} + \rho_g C_{v,g} \varepsilon_b \frac{\partial T}{\partial z} + \varepsilon_b P \frac{\partial u_{in}}{\partial z} + h_{gs} a_p (T - T_s) + \frac{2h_{gw}}{R_{in}} (T - T_w) = 0 \qquad (3)$$

where $k$ is the bulk gas phase thermal conductivity, $C_{v,g}$ is a constant volume molar heat capacity of the gas mixture, assumed to be a constant, $\rho_g$ is the molar density of the bulk gas, $a_p$ is the specific pallet surface per unit volume adsorber, $h_{gs}$ is the heat transfer coefficient between the gas and the solid phases, and $h_{gw}$ is the heat transfer coefficient between the gas phase and the adsorber wall. In this case, the factor of $2/R_{in}$, where $R_{in}$ is the inner radius of the adsorber, comes from the ratio of the circumference to the cross-sectional area of the adsorber. Also, notice that we have three different

temperature variables: the bulk gas temperature $\boldsymbol{T}$, the overall temperature of the solid adsorbent and the adsorbed species $\boldsymbol{T_s}$ , and the adsorber wall temperature $\boldsymbol{T_w}$.

The energy balance in the solid phase is given by:

$$\boldsymbol{\rho_b C_{p,s} \frac{\partial T_s}{\partial t} + \rho_b \sum_{i=1}^{ns} [ - \lambda_i(q,T) \frac{\partial q_i}{\partial t} ] + h_{gs} a_p (T - T_s) = 0} \qquad (4)$$

where $\boldsymbol{\rho_b}$ is the density of the solid adsorbent pallet, $\boldsymbol{C_{p,s}}$ is the heat capacity of the solid adsorbent, $\boldsymbol{\lambda_i(q,T)}$ is the isosteric heat of adsorption for the species, $\boldsymbol{a_p}$ is the specific pallet surface per unit volume adsorber, and $\boldsymbol{h_{gs}}$ is the heat transfer coefficient between the gas and the solid phases.

For the column wall, the energy balance is described by :

$$\boldsymbol{-k_w \frac{\partial {T_w}^2}{\partial z^2} + \rho_w C_{p,w} \frac{\partial T_w}{\partial t} - h_{gw} [ \frac{2R_{in}}{{R_{out}}^2 - {R_{in}}^2} ](T - T_w) + h_{wa} [ \frac{2R_{out}}{{R_{out}}^2 - {R_{in}}^2} ] ( T_w - T_{amb}) = 0} \qquad (5)$$

where $\boldsymbol{k_w}$ is the thermal conductivity of the adsorber wall, $\boldsymbol{\rho_w}$ is the density of the adsorber wall, $\boldsymbol{C_{p,w}}$ is the constant pressure heat capacity of the adsorber wall, $\boldsymbol{h_{gw}}$ is the interior heat transfer coefficient, $\boldsymbol{h_{wa}}$ is the exterior heat transfer coefficient.

An industrial adsorption unit experiences significant axial pressure drop during its operation when it operates with high-pressure feed conditions. The effect becomes most evident in systems with long adsorption columns because height relations to diameter (Lc/Dc>20) make uniform pressure distribution along the axis inadmissible. Pressure variations need explicit consideration in adsorption modelling because axial pressure distribution is not uniform in these situations. Pressure changes within Pressure Swing Adsorption (PSA) processes occur dynamically throughout the pressure swing steps. The correct depiction of this phenomenon requires a detailed pressure-flow relationship which needs inclusion within the complete Partial Differential Equations (PDEs) system modelling the adsorption process. The derivation of momentum balance equations from first principles exists to describe flow behaviour but empirical correlations serve preferred practical applications. Empirical models serve as computationally efficient tools that provide accurate pressure drop estimates in packed bed adsorbers which explains their widespread adoption across industrial-scale simulations. One of the most used empirical model is the Ergun equation [22] that is used to describe the pressure-flow relationship inside a packed bed adsorber and it can be written as:

$$\boldsymbol{-\frac{\partial P}{\partial z} = (1.50 \text{ x } 10^2) \frac{\mu_g}{D_p^2} \frac{(1-\varepsilon_b)^2}{\varepsilon_b^3} u_s + (1.75 \text{ x } 10^0) \frac{\rho_g}{D_p} \frac{(1-\varepsilon_b)}{\varepsilon_b^3} u_s |u_s|} \qquad (6)$$

where the pressure variables are in P, $\boldsymbol{u_s}$ is the superficial velocity, $\boldsymbol{D_p}$ is the diameter of spherical pellet, $\boldsymbol{\mu_g}$ is a constant viscosity of an ideal gas mixtures and $\boldsymbol{\rho_g}$ is the bulk density of a gas mixture.

### 2.2.3 Adsorption kinetics

The Linear Driving Force (LDF) model is one of the most commonly used models to describe the adsorption dynamics in both gas and liquid phases, particularly for the simulation of the cyclic sorption processes [23]. This model provides a more computationally efficient way of describing diffusion in sorbent particles than other, more complex methods that use partial differential equations (PDEs).

Fixed bed adsorber design and optimisation require mathematical models which allow researchers to perform multiple simulations to explore how different operating conditions impact system performance. The operation of a fixed bed adsorber is mainly governed by mass, energy and momentum balances which are described by partial differential equations. Different mathematical representations including pore diffusion model, pore and surface and homogeneous solid diffusion models explain mass transfer mechanisms through direct representation of spatial coordinates within the particle phase. The overall mass transfer resistance in these frameworks includes both external and intraparticle diffusive resistances, which provide a detailed description of the adsorption kinetics.

On the other hand, the LDF model simplifies the adsorption process by defining the uptake rate as being directly proportional to the difference between the time-averaged solute concentration inside the particle and the solute equilibrium concentration in the contiguous fluid phase. This approach greatly reduces the computational expense, which makes it suitable for large process simulations. In mathematical form, the equation of LDF is:

$$\frac{\partial q}{\partial t} = k\,(q_e - q\,) \tag{7}$$

where $q$ is the concentration of solute in the solid phase of adsorbent, $q_e$ concentration of solute in the solid phase of adsorbent in equilibrium and k is linear driving force mass transfer coefficient.

A significant characteristic of the LDF model is its consolidation of all mass transfer resistance, include both external film resistance and intraparticle diffusion resistance, into a single mass transfer coefficient, **k**. This coefficient governs the overall adsorption kinetics and is frequently determined empirically or inferred from comprehensive diffusion models.

Because of its simplicity, the LDF model is widely used in adsorption research to obtain accurate estimates of adsorption rates with a view to preserving computational efficiency. Due to its effectiveness, it is particularly suited to modelling pressure swing adsorption (PSA) and other cyclic operations for which rapid simulations are important for the optimisation of system performance.

## 2.3 Adsorbent materials

For the Pressure Swing Application, different classes of adsorbents are characterized by the benefits they have and the short comings that they are faced with. Picking the best suitable adsorbent is the result of the many factors including CO2 adsorption capacity, selectivity, stability under real operating conditions, resistance to water vapor, and ease of regeneration.

In the case of PSA, the very first and the most preferred materials were the zeolites, owing to their microporous structure and strong electrostatic interactions with CO2 molecules. Zeolite 13X is one of the best known and it is used all over due to the fact that it is the best at it. It gets very good adsorption capacities at low pressures and that is the reason why it has high CO2 selectivity [24]. Some works also point out zeolite 5A as one of the adsorbents [25]. The material also has high volumetric capacities and at the same time, the heat effects of adsorption are greatly reduced. However, the most severe drawbacks of these materials are that they are highly hydrophilic, which means that they are both highly sensitive to the presence of water vapor from flue gases and are also hydrophobic, the coin of the corresponding reverse.

Research into transcending the limitations placed by zeolites has revealed that Metal Organic Frameworks (MOFs), a fresh class of hybrid porous materials possess the potential to address these challenges because they have intrinsic porosity which arises from metal clusters combined with organic linker coordination [26]. The use of these materials has opened up the possibility to build professional building designs that allow for the environmental atmosphere to be balanced through selective venting. It should also be noted that in such systems, these materials allow for the CO2 adsorption, even if the atmosphere contains some water vapor. Moreover, Functionalized MOFs have not been only the latest advance in the CO2 capture technology, but they are also produced with higher selectivity than other materials of this kind. By the way, it is of course true because adsorption and desorption are associated with microstructure loss and iron and acid rains are added to the mix.

Activated carbon is part of a less advanced absorbent category that still holds some value and even though it lacks the selectivity of zeolites or MOFs it is popular due to its low cost, hydrophobic nature and the ability to be regenerated [27]. Zeolites are totally different from activated carbon materials, thus they are not affected much by water vapour and therefore will be more resistant to humid conditions in flue gases. Their adsorption capacity is moderate but they are quite durable and inexpensive, so they are still a feasible solution for industrial CO2 capture. The major disadvantage of activated carbons is that they have large pore size which leads to an inadequate CO2 separation efficiency. Nevertheless, functionalized carbon materials as well as hybrid composites that combine activated carbon with other porous structures have displayed higher activity and could be considered as a potential substitute to PSA-based separations.

The choice of appropriate adsorbent will be dependent on the particular process requirements of the substances to be separated and the properties of the substances in question. The type to be chosen will affect the performance in terms of the separation efficiency, total energy consumption, and finally the cost of the separation operation. In the ability to absorb $CO_2$, they are good for a certain amount of time; however, the best qualities of those elements are that they can be produced in large quantities and at low costs, and they are therefore effective for capturing $CO_2$ for large scale usage. In the study

of the detailed issues of absorbents, researchers have focused on the synthesis of hybrid and new materials that combine the advantages of different adsorption mechanisms.

This means that the choice of the adsorbent depends to a large extent on the application to which it is to be put as well as the nature of the substances to be separated. The kind approved will affect the following elements like the separation efficiency, energy consumption, and the price of the process itself.

## 2.4 TSA and VPSA systems

The main adsorption physical processes are Pressure Swing Adsorption and two other separation systems, namely Temperature Swing Adsorption (TSA) and Vacuum Pressure Swing Adsorption (VPSA). Temperature Swing Adsorption (TSA) has been patented and used for natural gas purification since the 1950s. Over the years, continuous improvements have resulted in several configurations being available. The TSA process can be seen in industrial plants that use either traditional fixed bed systems with two or three vessels or innovative configurations that combine TSA with multiple regeneration steps. The TSA process is especially used for natural gas dehydration, taking advantage of the temperature changes [28]. At low temperatures the target gas is adsorbed onto the adsorbent; thereafter desorption is induced by heating the adsorbent and the recovered gas is desorbed. For example, in a dual bed system, the first bed is supplied with wet gas flowing from top to bottom and dehydrated gas is produced at the outlet from the bottom. Finally, the second bed undergoes a desorption cycle and is regenerated by a hot regeneration gas counter currently (from bottom to top). The regeneration gas is pre-heated to the desired process temperature by a heat exchanger and is subsequently used to pre-heat the fixed beds to the adsorption temperature. Now that systems are being used for economic reasons, four or more fixed beds are used to guarantee that product gas flow is not interrupted. It allows desorption in some cases but thermal cycles are generally slower and may lead to higher energy usage for heating and cooling.

VSA operates on the same principle as PSA but uses a vacuum to desorb instead of pressure. In VSA, desorption is done by reducing the pressure to below atmospheric to create a vacuum [29]. Vacuum use improves gas recovery while specifying higher product gas purity standards but requires additional equipment for vacuum operation.

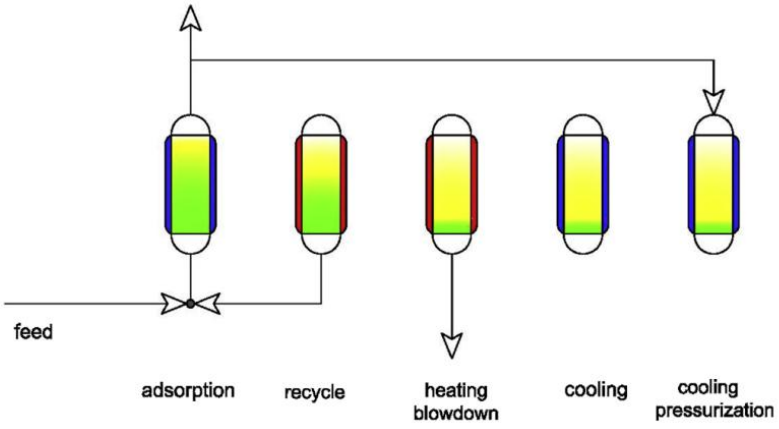


*Figure 2.3 Schematic diagram of a TSA cycle*

## 2.5 Performance Metrics

PSA process offers a very high flexibility in design, in fact, a totally different number of columns can be used and also a fairly large number of cycles are possible. To be able to evaluate a certain implementation of PSA and to understand the behaviour of PSA, some indicators are defined in order to measure how well the system is performing. The standard performance metrics for PSA processes are product purity, product recovery, productivity, and energy consumption [21].

For a product stream, e.g., the raffinate or the extract, the product purity of species *i* is the averaged mole fraction of species *i* in the total amount of the product harnessed by the product stream during a PSA cycle, i.e., the throughput. Product recovery is defined for each species *i* as well. The product recovery of species *i* is defined as the ratio between the total amount of species *i* produced in the PSA cycle divided by the total amount of species *i* fed into the PSA network as a part of the feed stream. The productivity of a product stream can be defined as the total amount of the product generated in a product stream divided by the product of the duration of the PSA cycle and the mass of the adsorbent. Finally, the energy consumption can be defined as the total amount of energy expended due to the compression and vacuum work during the PSA cycle. A summary of the equations for the Performance Metrics is:

| Performance Metrics | Equation | |
|---|---|---|
| *Purity ( $i^{th}$ species )* | $\frac{mol\ i^{th}\ specie\ in\ raff.(extr.)}{total\ mol\ i^{th}\ specie\ fed\ in\ cycle\ time}$ | (8) |
| *Recovery ( $i^{th}$ species )* | $\frac{mol\ i^{th} in\ raff.(extr.)}{\sum mol\ i^{th} species\ in\ feed}$ | (9) |
| *Raff./Extr. Productivity* | $\frac{mol\ i^{th} in\ raff.(extr.)}{m_{ads} \cdot t_{cycle}}$ | (10) |

*Table 3.1 – Summary of performance metrics*

# CHAPTER 3: WATER ELECTROLYSIS and METHANATION PROCESS

Water electrolysis is the simplest way for producing green hydrogen. It permits to store the overproduction of electricity in a chemical form for long terms. With alkaline water electrolysis is intended the concept of using electricity for splitting the water molecule into oxygen and hydrogen using an alkaline solution as electrolyte. It is usually performed below 100°C and a maximum pressure of 32 bar because of the liquid form of the electrolyte. Using a polymer membrane as electrolyte makes it possible to reach higher temperatures and a better dynamic behaviour (PEM). Higher temperatures could be reached using solid oxide as electrolyte, increasing the efficiency of the process (SOEC).

The electrochemical cell is the fundamental component of an electrolyzer, it is composed of an electrode acting as anode and an electrode acting as cathode; they are connected by means of an external electric circuit and they are submerged in the electrolyte bath. A membrane act as a solid separator between the two electrochemical parts, avoiding the diffusion of O2 and H2 gas molecules. The potential of a single cell is limited, so different cells are connected in series forming stacks, and different stacks could be further connected together, to form the electrolyzer. The voltage imposed depends on the characteristics of the cell and the hydrogen production rate is proportional to the current density.

## 3.1 Electrolyzer technology

Water splitting in its simplest form uses an electrical current passing through two electrodes to break water into hydrogen and oxygen. This type of reactions is not spontaneous and so requires a level of energy to occur, accordingly they are also defined as endothermic. Electrolysis technologies are usually grouped in two categories according to the temperature of operation. The low temperature technologies are the Alkaline electrolyzers and the Proton-exchange membrane electrolyzsers, while the high temperature ones are represented by the Solid oxide electrolyzers. The most common electrolysis technology is alkaline based, but more proton exchange membrane electrolysis and solid oxide electrolysis cells units are developing. SOEC electrolyzers are the most electrically efficient, but are the least developed of the technologies. SOEC technology has challenges with corrosion, seals, thermal cycling, and chrome migration. PEM electrolyzers are more efficient than alkaline, do not have the corrosion and seals issues that SOEC, but cost more than alkaline systems. Alkaline systems are the most developed and lowest in capital cost [30].

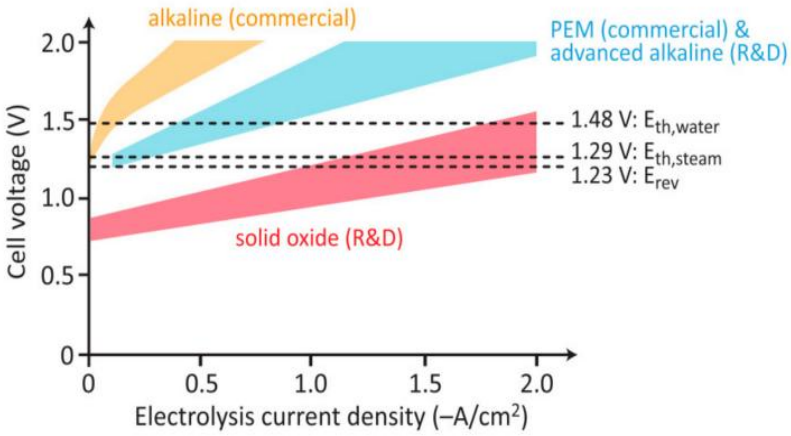


*Figure 3.1 – Comparison between different electrolyzers [31]*

### 3.1.1 Akaline water electrolysis (AWE)

Hydrogen production by alkaline water electrolysis is by a well-established technology with an efficiency around 50-60% [32]. The electrochemical semi-reactions that occurs on the electrodes are:

- Cathode: $2H_2O\ (l) + 2e^- \rightarrow H_2(g) + 2OH^-(aq)$
- Anode: $2OH^-(aq) \rightarrow 2e^- + \frac{1}{2}O_2(g) + H_2O\ (l)$

This electrolyzer is characterized by having two electrodes operating in a liquid alkaline electrolyte solution, generally potassium or sodium hydroxide (KOH or NaOH), the electrodes are kept apart by a diaphragm, where the transport of the hydroxide ions ($OH^-$) occurs, from one electrode to the other. So, the process initiates at the cathode, the site of reduction, where two molecules of an alkaline water solution are reduced to one molecule of hydrogen ($H_2$), and two hydroxyl ions are produced ($OH^-$). The produced hydrogen emanates from the cathode surface to recombine in a gaseous form, while the hydroxyl ions transfer through the porous diaphragm to the anode, under the influence of the imposed electrical potential. Here a similar reaction occurs: two water molecules are oxidized, forming one diatomic oxygen ($O_2$) molecule and four hydrogen atoms.

In alkaline electrolysis systems run at low temperatures ranging from 30 to 80°C and utilize a water based solution as the electrolyte fluid medium for the process to occur smoothly. The separator or diaphragms commonly employed are permeable to avoid any blending of resultant gases and to keep the nickel electrodes isolated from each other. The diaphragmatic barrier situated in the center of the cell acts as a partition, between the cathodic and anodic regions, within the system. This approach does come with a drawbacks, like restricted capacities and reduced operational pressure and energy efficiency levels, characteristics that make this particular type of electrolyzer better suited for consistent power operation when linked to the grid. One notable advantage of alkaline cells lies in the cost option to replace cells instead of the entire stack as seen in other cell variants. Moreover alkaline electrolyzers boast a durability factor offering an operational lifespan ranging from 10 to 20 years [33]. Research in the sector has the goal of an increase in operating pressure and temperature. Increasing temperature has advantage related to reaction kinetics.

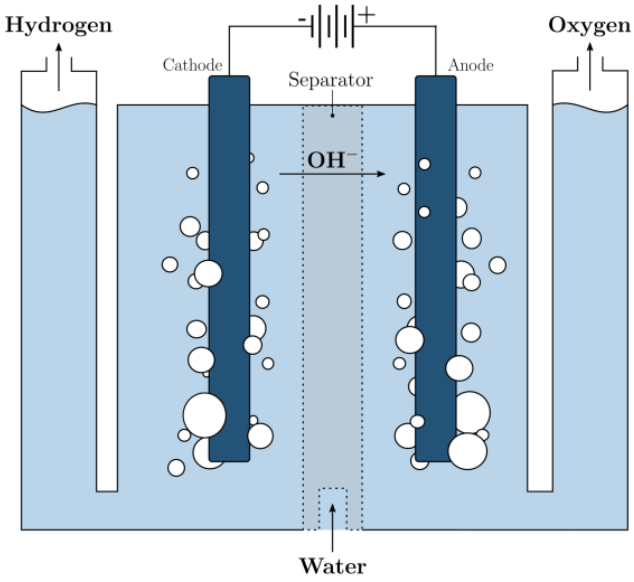


*Figure 3.2 - Schematic illustration of an alkaline water electrolyzer [32]*

### 3.1.2 Proton Exchange Membrane Water Electrolysis (PEMWE)

This technology of electrolyzers perform water electrolysis trough proton exchange membrane electrolyte made by Nafion and the following electrode reactions take place:

- Cathode: $2H^+(aq) + 2e^- \rightarrow H_2(g)$
- Anode: $H_2O(l) \rightarrow 2H^+(aq) + 2e^- + \frac{1}{2}O_2(g)$

These proton exchange membranes are very important because they have low gas permeability, high proton conductivity, are thin and can be used at high pressures and ambient temperatures. They have an efficiency of 60-80%. In terms of sustainability and environmental impact, is also found to be one of the most favourable methods of conversion of renewable energy to highly pure hydrogen. This is mainly due to other promising advantages like it's compact design, high current density, higher efficiencies, fast response and small footprint. Electrocatalysts used in this method are usually noble metals such as platinum or palladium for the cathode and iridium or ruthenium oxide for the anode which makes the whole process more expensive than alkaline water electrolysis. In this process water is pumped onto the anode where it is electrochemically split into oxygen, hydrogen, protons and single electrons; these protons then travel via the proton exchange membrane to the cathode side while the electrons exit from the anode through the external power circuit which provides the driving force to the chemical reaction. In result, the major challenge of proton exchange membrane water electrolysis is to improve the production cost without compromising the efficiency [32].

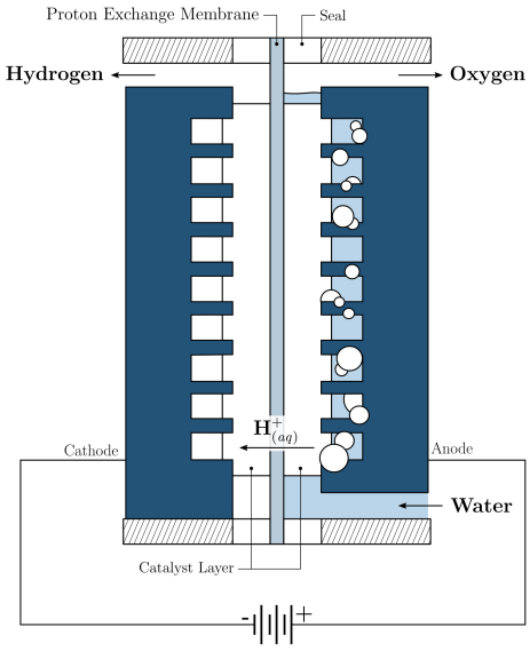


*Figure 3.3 - Schematic illustration of a proton-exchange membrane water electrolyzer [32]*

### 3.1.3 Solid Oxide Electrolysis (SOEC)

This method has attracted significant attention due to the conversion process of electrical into chemical energy, along with the high-efficiency production of pure hydrogen. Solid oxide electrolysis operates at high pressures and temperatures, being novel by using water in the form of steam [32]. The reactions are:

- Cathode: $H_2O + 2e^- \rightarrow H_2 + O^{2-}$
- Anode: $O^{2-} \rightarrow 2e^- + \frac{1}{2}O_2$

Solid oxide electrolysis cells or SOECs are, like oxide fuel cells. Working in reverse mode, where they use thermal energy to help split water along with electrical energy making the process more efficient by reducing power loss due to overpotentials at the anode and cathode thus cutting down the electricity needed by, around 35%. In a SOEC system oxygen ions move through the electrolyte while leaving hydrogen in steam that has not reacted resembling how an alkaline system functions. High temperature electrolysis using an oxide based electrolyzer offers benefits such, as employing a solid electrolyte that is non corrosive compared to KOH used in alkaline systems and avoids issues with liquid flow distribution problems typically encountered in other systems. However operating at temperatures necessitates the use of materials and fabrication techniques as well, as a heat source. The components are quite similar, to those under development for oxide fuel cells (SOFC) like yttria stabilized zirconia (YSK) electrolyte and a nickel containing YSK anode along, with metal doped

lanthanum metal oxides that are facing similar seal related challenges being studied currently. The effectiveness of high temperature electrolysis is heavily influenced by the temperature and the heat source utilized in the process itself. Moreover it's worth noting that the efficiency based as a function of input can reach remarkably high levels ranging between 85 90% [30].

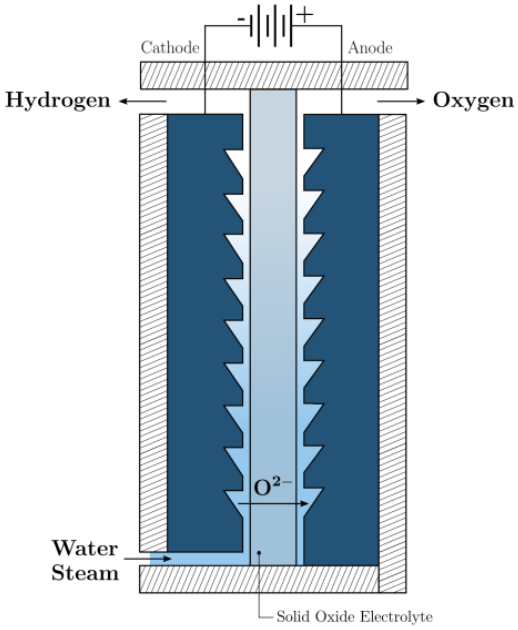


*Figure 3.4 - Schematic illustration of a solid oxide water electrolyzer [32]*

## 3.2 Fundamentals on electrolysis

The electrolysis cell is the fundamental device which makes it possible to transform water into hydrogen and oxygen. This is possible following the reaction:

$$H_2O + electrical\ energy \rightarrow H_2 + \frac{1}{2} O_2 \qquad (11)$$

The water splitting reaction shows a variation of the Gibbs free energy positive ($\Delta G° = +237$ kJ/mol at standard condition), which means that the reaction is non-spontaneous and an external energy source must be applied to make it happen. The energy is applied in the form of electricity, as a potential through the electrodes submerged in the aqueous solution [34]. A schematic design is illustrated in 3.5, where it is also possible to see the two half reactions at the anodic and cathodic side.

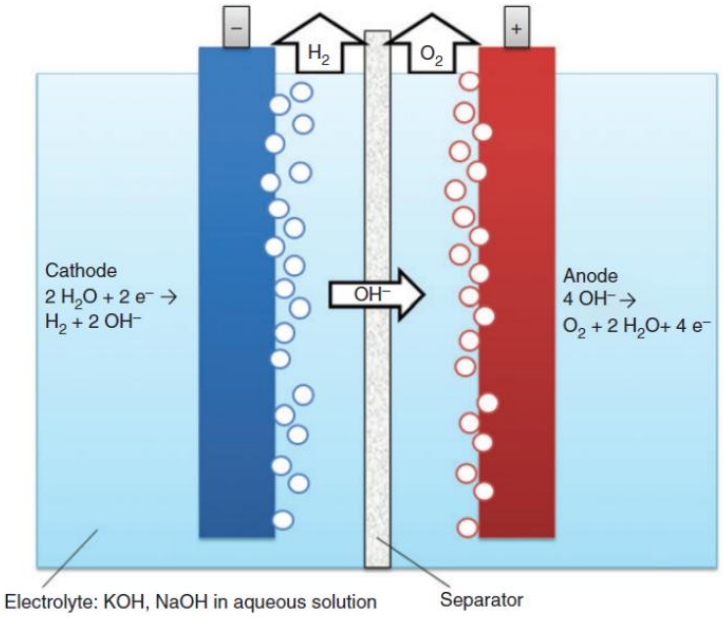


*Figure 3.5 - Schematic representation of an alkaline electrolysis cell*

The fundamental components are anode, cathode, electrolyte and separator. When an external DC source is applied, the electrons are consumed by water molecule ($H_2O$) to form hydrogen. In order to balance the electrical charge, the hydroxide ions ($OH^-$) transfer through the separator, releasing the electron at the anode. The electrolyte is a solution consisting of water, and salt to improve the conductivity of ions. The concentration of salt, in the solution, increases the conductivity, which consequently increases the corrosion of the metal electrodes. The diaphragm act as a solid separator, in order to not mix the hydrogen and oxygen produced in the gas form.

The cathode and anode sub-reactions, respectively, can be defined as:

$$H_2O + 2e^- \rightarrow H_2 + 2OH^- \tag{12}$$

$$2OH^- \rightarrow \frac{1}{2}\,O_2 + H_2O + 2e^- \tag{13}$$

## 3.3 Thermodynamic model

The operations of an electrochemical cell could be described by means of fundamentals thermodynamics. An electrolyzer works converting electrical energy into chemical energy, in the form of hydrogen. The following assumptions can be made about the water splitting reaction: hydrogen and oxygen are ideal gases, water is an incompressible fluid, and the gas and liquid phases are separate. Based on these assumptions the change in enthalpy ΔH, entropy ΔS, and Gibbs energy ΔG of the water splitting reaction can be calculated with reference to pure hydrogen ($H_2$), oxygen ($O_2$),

and water ($H_2O$) at standard temperature and pressure (25°C and 1 bar). The total change in enthalpy for splitting water is the enthalpy difference between the products ($H_2$ and $O_2$) and the reactants ($H_2O$). Considering an electrochemical cell operating at constant temperature and pressure, the energy requirements for the water electrolysis reaction is represented by the enthalpy of formation ΔH. The same applies for the total change in entropy. It could be seen as the sum of two contributions: one electrical and the other in form of heat. The electrical contribution is defined as the change in Gibbs free energy ΔG. The thermal energy Q could be described as the product between the temperature at which the reaction occurs and the entropy change ΔS [35]. In mathematical form:

$$\Delta G = \Delta H - Q = \Delta H - T \cdot \Delta S \tag{14}$$

The sign of the Gibbs free energy determines the spontaneity of the reaction, while the enthalpy variation determines the thermal requirements. The process that occurs in a electrochemical cell is endothermic (ΔH > 0) and non-spontaneous (ΔG > 0). The reversible cell voltage $V_{rev}$ is the lowest required voltage for the electrolysis to take place. This voltage can be expressed as a function of G by means of:

$$V_{rev} = \frac{\Delta G}{z \cdot F} \tag{15}$$

where z is the number of electron moles transferred per hydrogen mole (z = 2) and F is the Faraday constant, which represents the charge on one mole of electrons (96.485 C/mol). If the thermal energy T · ΔS is provided by means of electricity, as is the case in most commercial electrolysers, the minimum voltage for water electrolysis to occur is known as the thermo-neutral voltage $V_{tn}$. In an ideal electrolysis process, $V_{tn}$ is equal to the enthalpy voltage $V_{\Delta H}$ since the total energy required is equal to the enthalpy change $\Delta H$. In this case, both $V_{\Delta H}$ and $V_{tn}$ can be obtained from the following expression:

$$V_{tn} = \frac{\Delta H}{z \cdot F} \tag{16}$$

However, in a real electrolysis process, $V_{tn} > V_{\Delta H}$. The reason is the additional energy consumption, both electric and thermal, caused by thermodynamic irreversibilities that are mainly related to the water vapor contained in the hydrogen and oxygen flows, the lower temperature and pressure of the supply water with respect to the operation set-points, and the fact that the process is not actually adiabatic, hence entitling thermal losses due to convection and radiation. At standard conditions $V_{rev}$ =1.23 V and $V_{tn}$ =1.481, but these will change with temperature and pressure.

## 3.4 Electrochemical model

When applying a DC current on the two end of an electrolyzer, the voltage of the cell experiences an increase, with the respect to the open circuit condition which is the voltage when the current flow is zero [35]. This phenomenon is mainly caused by different irreversible processes, such as overvoltages and parasitic currents, which generate energy losses limiting the cell efficiency. In order to maximize the hydrogen production with minimal amount of energy, it is important to understand all these

phenomena affecting the operating voltage of an electrochemical cell. It is also necessary to investigate the effect of operating parameters and device design in the formation of overvoltages.

The Ulleberg model is able to predict the electrochemical behaviour of an alkaline water electrolysis stack under different operating conditions, such as, temperature (T) and subsequently pressure (p) [36]. Equations are used to determine polarization curve, faraday efficiency and gas purity as a function of current based on both physical principles of the electrolysis process and statistical data. The polarization curve is the plot of the current (I) versus the voltage ($V_{cell}$) of the cell. It is a very useful tool to help understand an electrolytic cell. All curves are specific to temperature, pressure and kind of cell chosen.

### 3.4.1 Polarization curve

The polarization curve analyzes, to determine the cell voltage as a function of current density, the different overpotentials that are occurring during the electrolysis of water. At standard conditions (25°C and 1 bar), a minimum voltage is required for the reaction to occur, this is referred to the reversible voltage, and is 1.23 V.

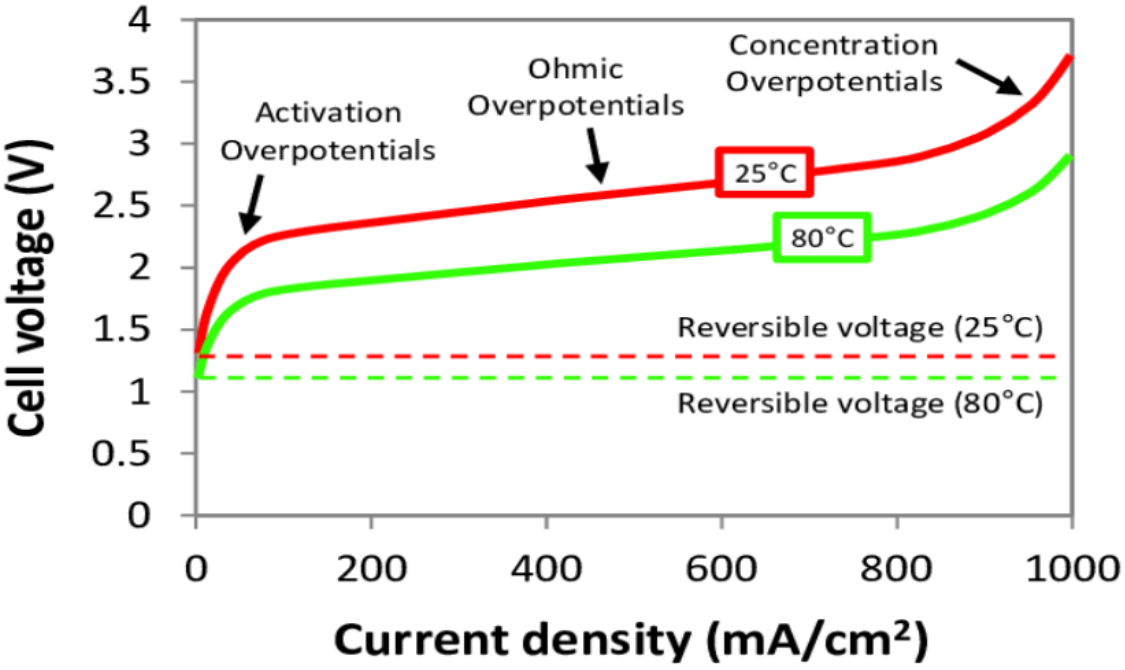


*Figure 3.6 – Polarization curve of an alkaline electrolysis cell at different temperatures [37]*

However, the cell voltage is always higher than theoretical one by the appearance of a series of overpotentials due to kinetic and resistive effects. So the real cell voltage can be defined as the sum of reversible voltage and each of these overpotentials ($\hat{\eta}$), activation overvoltages ($\hat{\eta}_{an}$, $\hat{\eta}_{cat}$), ohmic overpotentials ($\hat{\eta}_{ohm}$) and concentration overpotentials ($\hat{\eta}_{conc}$), as shown in the following equation [38]:

$$V_{cell} = V_{rev} + \hat{\eta}_{an} + \hat{\eta}_{cat} + \hat{\eta}_{ohm} + \hat{\eta}_{conc} \quad (17)$$

The so-called ohmic losses result in the term $\hat{\eta}_{ohm}$. First, these losses are due to the resistance of several cell elements (electrodes, current collectors, interconnections etc.) to electron flow. They are also attributed to the resistance to the ionic flow of the electrolyte, the gas bubbles, and the diaphragm. Furthermore, $\hat{\eta}_{ohm}$ is mainly a function of the electric current passing through the cell. The activation overvoltage, denoted by $\hat{\eta}_{act}$, is ascribed to electrode kinetics. To effect charge transfer between the chemicals and the electrodes requires energy. This energy barrier which the charge must overcome to move from the reactants to the electrodes and back again depends sensitively on the catalytic nature of the electrode materials. It results in an overvoltage across the electrodes denoted by $\hat{\eta}_{act}$. The anodic half reaction suffers from a much higher activation overvoltage than the cathodic half reaction. The concentration overvoltage, denoted by $\hat{\eta}_{conc}$, is caused by mass transport processes (convection and diffusion). Diffusion and convection rate limit the availability of reactants while enhancing the concentration of the products at the electrode electrolyte interface. Usually, $\hat{\eta}_{conc}$ is much lower than $\hat{\eta}_{ohm}$and $\hat{\eta}_{act}$, especially in the case of alkaline electrolysis [35].
The polarization curve can be determined using a semi-empirical model. In this regard, one of the most widely used models to describe the electrochemical response of an electrolyzer is proposed by Ulleberg in 2003 and it is based on a combination of fundamental thermodynamics and empirical electrochemical relationships, as in the following manner:

$$V_{cell} = V_{rev} + r \cdot i + s \log [t \cdot i + 1] \quad (18)$$

In Eq. (18), the first term represents the reversible voltage, which can be determined by the change in Gibbs energy. The second term is related to ohmic overpotentials by r. Finally, the activation overpotentials are defined through the parameters s and t. The parameter s is commonly assumed as a constant value and t and r coefficients are described as a function of the temperature (T) by respectively:

$$t = t_1 + \frac{t_2}{T} + \frac{t_3}{T^2} \quad (19)$$

$$r = r_1 + r_2 \cdot T \quad (20)$$

However, in this model, the polarization curve only depends on the temperature. In order to obtain a more comprehensive model, the equation is modified to include the pressure (p). For this purpose, an additional parameter d has been incorporated in the model. It represents the linear variation in the ohmic overpotentials according to the pressure:

$$d = d_1 + d_2 \cdot p \quad (21)$$

The Eq. (21) shows the final model proposed in this study for the polarization curve:

$$V_{cell} = V_{rev} + [(r_1 + d_1) + r_2 \cdot T + d_2 \cdot p\,] \cdot i + s \log\left[\left(t_1 + \frac{t_2}{T} + \frac{t_3}{T^2}\right) i + 1\right] \quad (21)$$

Where $r_1$, $r_2$, $d_1$, $d_2$, s, $t_1$, $t_2$ and $t_3$are constants showed in Table 3.1 [38]. Finally, the total voltage of the alkaline electrolyzer is equal to the cell voltage multiplied by the number of cells of the stack.

| Coefficient | Value | Unit |
|---|---|---|
| $r_1$ | 4.4153 x $10^{-5}$ | $\Omega\, m^2$ |
| $r_2$ | 6.88874 x $10^{-9}$ | $\Omega\, m^2\, °C^{-1}$ |
| $d_1$ | -3.12996 x $10^{-6}$ | $\Omega\, m^2$ |
| $d_2$ | 4.47137 x $10^{-7}$ | $\Omega\, m^2 bar^{-1}$ |
| $s$ | 0.33824 | V |
| $t_1$ | -0.01539 | $m^2\, A^{-1}$ |
| $t_2$ | 2.00181 | $m^2\, °C\, A^{-1}$ |
| $t_3$ | 15.24178 | $m^2\, °C^2 A^{-1}$ |

*Table 3.1 – Coefficients for polarization curve*

## 3.4.2 Faraday efficiency

The amount of gas produced by an electrochemical process can be related to the electrical charge consumed by the cell, which is described by Faraday's law. For an ideal water electrolysis system, the electric charge, passing through the cell, is a direct measure of the amount of hydrogen produced. From this, it is possible to measure the effectiveness of the real process by comparing the charges fed to the system and the amount of hydrogen produced [39]. This parameter, called Faraday efficiency ($\eta_f$), is defined as the ratio between the volume of gas produced in a given time interval ($Q_{exp}$) and the theoretical volume that should be produced during the same time ($Q_{th}$), in accordance with Faraday's law:

$$\eta_f = \frac{Q_{exp}}{Q_{th}} \quad (23)$$

In a similar way to the polarization curve, the Faraday's efficiency can be also modelled by an empirical expression for a given temperature using 4 parameters for this purpose such as Eq. (24) where the pressure has not included due to its slight influence:

$$\eta_f = \left(\frac{i^2}{f_{11} + f_{12} \cdot T + i^2}\right) \cdot (f_{21} + f_{22} \cdot T) \tag{24}$$

Where $f_{11}$, $f_{12}$, $f_{21}$ and $f_{22}$are constants from Table 3.2 [38].

| Coefficient | Value | Unit |
|---|---|---|
| $f_{11}$ | 478645.74 | $A\,m^{-4}$ |
| $f_{12}$ | -2953.15 | $A\,m^{-4}\,°C^{-1}$ |
| $f_{21}$ | 1.03960 | - |
| $f_{22}$ | -0.00207 | $°C^{-1}$ |

*Table 3.2 – Coefficients for Faraday efficiency*

### 3.4.3 Gas purity model

Renewable energy-driven electrolyzer highlights the importance of gas purity as a critical safety indicator. When the HTO reaches the safety limit (2%), the electrolyzer should be shut down to avoid the formation of a flammable gas mixture [40]. Gas purity at partial load is an important operating parameter, especially when the electrolyzer is powered by a renewable energy source. Two effects can be responsible for the contamination of the product gases with the respective other component (gas crossover) in the generation of hydrogen and oxygen in an electrolyzer. One source is the diffusion of gas through the diaphragms and seals with the cell block. This does not only decrease the gas quality, but also the overall electrical efficiency on the electrolyzer as oxygen can react back to water with hydrogen present at the cathode. The other source is the dissolution of small amounts of the gases ($H_2$ and $O_2$) in the liquid electrolyte, so each half of the electrolyte stream is saturated with the corresponding gas during electrolysis and the gas separator vessel cannot remove the dissolved gas but only the bubbles. At low current densities, the purity of the gases produced is significantly reduced. This is due to that the mentioned phenomena are mostly independent of the electrolyzer load, so the contamination of the products gases increases with low gas production rate because the percentage of total impurities is higher. Thereby, the contamination level is mainly dependent on operational parameters such as temperature, pressure, material properties of the diaphragm and process control. Finally, a model for the diffusion of hydrogen to oxygen (HTO) has been proposed in Eq. (25) considering the influence of temperature and pressure on the purity of the gases:

$$HTO = [C_1 + C_2 \cdot T + C_3 \cdot T^2 + (C_4 + C_5 \cdot T + C_6 \cdot T^2) \cdot \exp\left(\frac{C_7 + C_8 \cdot T + C_9 \cdot T^2}{i}\right)] \tag{25}$$

$$+ [E_1 + E_2 \cdot p + E_3 \cdot p^2 + (E_4 + E_5 \cdot p + E_6 \cdot p^2) \cdot \exp\left(\frac{E_7 + E_8 \cdot p + E_9 \cdot p^2}{i}\right)]$$

Among all the parameters $C_1$ to $C_9$ are constants that represent the influence of temperature in the HTO and $E_1$ to $E_9$ indicate the relation between the gas purity and the pressure. All the constants are shown in table 3.3.

| Coefficient | Value | Unit |
|---|---|---|
| $C_1$ | 0.09901 | - |
| $C_2$ | -0.000207 | $°C^{-1}$ |
| $C_3$ | 1.31064 x $10^{-5}$ | $°C^{-2}$ |
| $C_4$ | -0.08483 | - |
| $C_5$ | 0.00179 | $°C^{-1}$ |
| $C_6$ | -1.13390 x $10^{-5}$ | $°C^{-2}$ |
| $C_7$ | 1481.45 | $A\,m^2$ |
| $C_8$ | -23.60345 | $A\,m^2°C^{-1}$ |
| $C_9$ | -0.25774 | $A\,m^2°C^{-2}$ |
| $E_1$ | 3.71417 | - |
| $E_2$ | -0.93063 | $bar^{-1}$ |
| $E_3$ | 0.05817 | $bar^{-2}$ |
| $E_4$ | -3.72068 | - |
| $E_5$ | 0.93219 | $bar^{-1}$ |
| $E_6$ | -0.05826 | $bar^{-2}$ |
| $E_7$ | -18.38215 | $A\,m^2$ |
| $E_8$ | 5.87316 | $A\,m^2 bar^{-1}$ |
| $E_9$ | -0.46425 | $A\,m^2 bar^{-2}$ |

*Table 3.3 – Coefficients for Gas purity*

## 3.5 Principles of methanation

The technology of methanation, which allows to convert a generic syngas, a mixture of hydrogen and carbon monoxide, into Synthetic Natural Gas (SNG) is presented. The CO and $CO_2$ methanation techniques were discovered in 1902 by Paul Sabatier and Jean-Baptiste Senderens, and have been used in various applications for over 100 years [41]. By the two process the carbon monoxide and carbon dioxide can be converted to methane according to the following reactions:

$$CO + 3H_2 \rightleftharpoons CH_4 + H_2O \quad (26)$$

$$CO_2 + 4H_2 \rightleftharpoons CH_4 + 2H_2O \quad (27)$$

Both reactions are linked by the water gas shift conversion, which is always observed simultaneously whenever active catalysts are used:

$$CO + H_2O \rightleftharpoons CO_2 + H_2 \quad (28)$$

But when the methanation reaction occurs due to the realising heat there is a strong increase of temperature and as a consequence, in an exothermic reaction, an increase of temperature push toward the reagents the reaction. This can lead the reaction toward the reactants decreasing the degree of conversion and since the catalyst is a porous material, increasing the temperature can modify the grain size decreasing the specific surface leading to a degradation of catalyst bed.

The methanation process can be carried out in isothermal conditions or adiabatic conditions, and different reactor concepts (fixed beds, fluidized beds, three phase, and structured reactors) have been developed based on these approaches. In the next section TREMP™ ("Topsøe Recycle Energy-efficient Methanation Process") process will be analyzed. This process will be then modelled coupled to the alkaline electrolyzer.

### 3.5.1 $TREMP^{TM}$ process description

A significant issue in a methanation reactor is the temperature control in order to prevent thermodynamic limitation and catalyst sintering. Haldor Topsøe has reinitiated its efforts in the technology, and the knowledge gained over the years has been used to refine the tried and tested technology and catalyst [42]. Methanation has been employed for many years as the final filtration step in ammonia plants. However, methanation for the purpose of SNG production is at a different level due to the higher content of carbon monoxide and carbon dioxide. CO and $CO_2$ are hydrogenated according to the methanation reactions, both of which are favored by low water content and high pressure. Since the methanation reactions are the reverse of reforming reactions, and since reforming reactions are highly endothermic, it follows that they are also highly exothermic, for example, if a gas mixture is injected into an adiabatic methanation reactor at 300°C, the reaction can reach temperatures in excess of 900°C. The adiabatic temperature increase needs a catalyst that is also stable at high temperatures and yet active at low temperatures. In order to obtain at the end of the methanation step a product with more than 95% of methane, the methanation process has to be performed in more step, so more adiabatic reactors working at decreasing temperature levels and split

by intermediate cooling. The exact number of reactors is chosen considering a trade-off between product gas quality requirements and heat recovery.

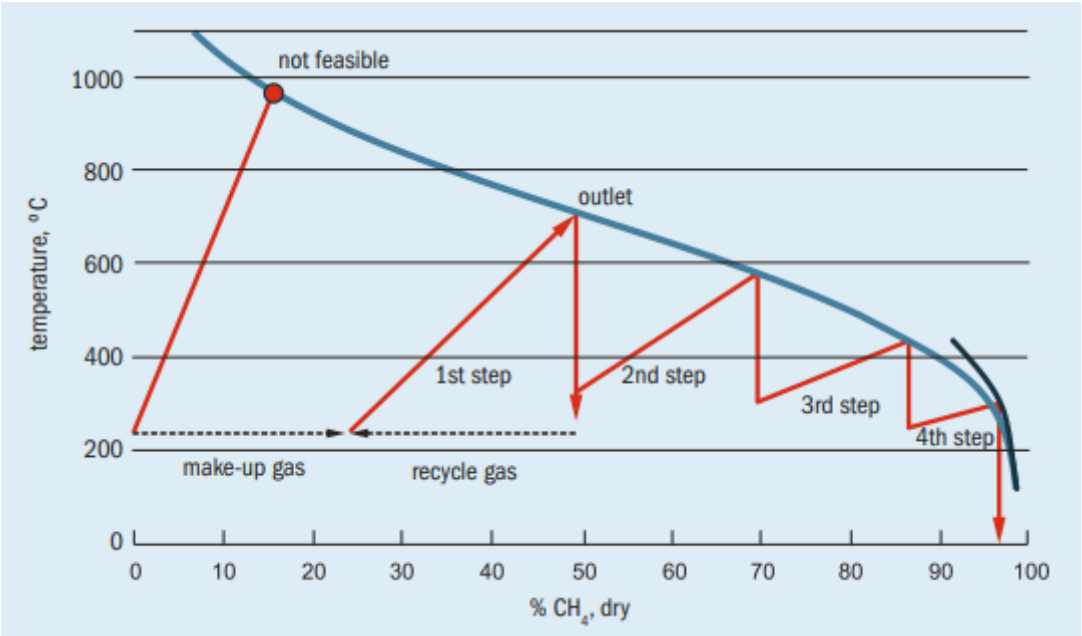


*Figure 3.8 – Equlibrium curve for methanation process [42]*

In Figure 3.9 a schematic of methanation using TREMP™ is shown. This technology addresses the essential question of minimum recycle cost and heat recovery in the most efficient manner by recovering the heat as high-pressure superheated steam. Based on the limitations and opportunities mentioned, TREMP™ works in the following way. The feed is first passed through a sulphur guard bed for removal of traces of sulphur components that have not been picked up by the upstream acid gas removal unit. The desulphurized feed is then mixed with recycle gas to control the maximum temperature rise and passed to the first methanation reactor. The exothermic methanation reaction results in a high outlet temperature, which allows the reaction heat to be recovered for generation of superheated high-pressure steam in the downstream heat exchangers. After cooling, the partly methanated syngas passes through two or three additional methanation reactors in series for complete conversion of the CO and/or CO2 into methane. The number of methanation reactors will depend on the operating conditions, such as pressure, as well as the SNG product specification. If number of reactors is high (four or more), there's also the possibility of an additional operation: before the last methanation step, the water generated in upstream methanation steps can be removed in order to push the equilibrium further towards methane production. The process stream leaving the last methanation reactor is cooled, dried, compressed and eventually corrected to meet the pipeline specifications or LNG production requirements. The methanation reaction is favored by high pressure, and works well with syngas from all types of coal or biomass gasifiers [42].

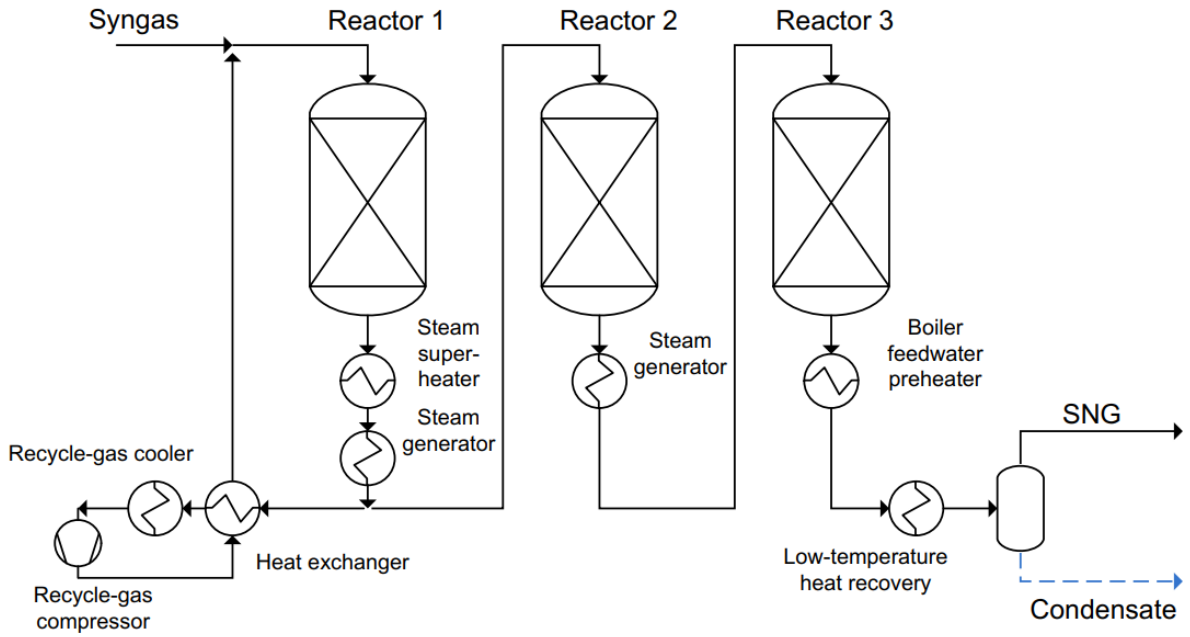


*Figure 3.9 - TREMP™ methanation process [43]*

The TREMP™ technology produces a natural gas compatible with pipeline specifications, ensuring easy distribution of the product. Generally, the SNG produced by TREMP™ coupled with gasification of solid fuels is composed by methane (94-98%), hydrogen (0,05-2%), carbon dioxide (0,2-2%), carbon monoxide (<100ppm), Nitrogen and Argon (2-3%).

# CHAPTER 4: MODEL AND RESULTS

After the theoretical study carried out in the previous chapters where pressure swing adsorption, water electrolysis and methanation are studied from the thermodynamic and chemical point of view, in this chapter it is discuss in detail their modelling.

The pressure swing adsorption system simulates the biogas upgrading, with focus on the $CO_2$ captured which is then used integrating with hydrogen production to produce Synthetic Natural gas. The PSA process is based on the following assumptions: isothermal operation, no axial pressure drop, flow driven and Linear Driving Force kinetic.

The alkaline electrolyzer is modelled according to Ulleberg model equation in order to evaluate the performance at different working conditions but with the respect of $H_2/CO_2$ ratio equal to 4 considering a faraday efficiency unitary.

Then the electrolyzer and the methanation reactors are built using the software Aspen Plus.

In the end, an economic analysis is performed because is very useful to compare different configurations of the methanation production plant, because the price of the product clearly explains the economic competitiveness of the process. Both the capital and the operating costs of the P2G plant are estimated, the information necessary for the quantification of costs are mainly obtained from the literature. Considering capital and annual costs allows to build a detailed cash flow analysis. In this work plant capital and annual costs have been considered in order to build a detailed cash flow analysis. Annual costs account for operating and maintenance items, energy input as well as material streams input cost.

## 4.1 Pressure Swing Adsorption configuration

In this section is analyzed the PSA system for the carbon capture from a biogas feed gas evaluating the different behaviour according to the influencing parameters. It's possible to simulate the PSA system using toPSAil, through the MATLAB code, with the presence of two adsorption columns connected with a feed tank and two product tanks through a network of pipes, valves, and pumps. There are three flow sections :

- *Feed section*: contains the feed compressor C-1, the feed heat exchanger H-1, the pressure controller V-1, and the feed tank T-1. The compressor raises the feed pressure to a desired value $P_f$, after which the heat exchanger adjusts the temperature to the desired value but we neglect the heating or cooling requirement in H-1 and assume that the desired feed condition is achieved exactly before the feed stream enters the feed tank.
- *Raffinate section*: raffinate product from the adsorbers is either discarded and collected in T-2;
- *Extract section*: raffinate product from the adsorbers is discarded or sent to T-3;

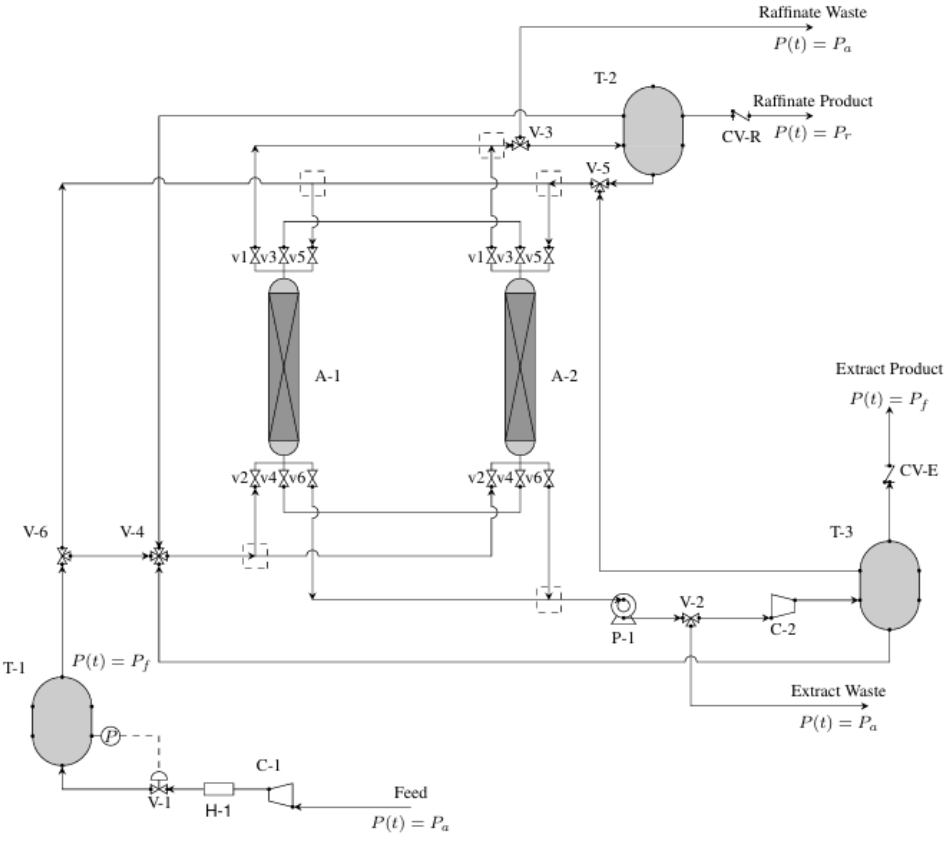


*Figure 4.1 – Process Flow Diagram of PSA*

The adsorber network consists of the adsorbers (A-1 and A-2) and their associated valves. Each adsorber has six valves (v1–v6) associated with it. Even numbered valves are at the feed end, while odd numbered valves are at the product end. At most one valve is open at each end at any time, and the pressure-flow relationship for the open valve is determined by the choice of the boundary conditions discussed in Section 3.1.9. An adsorber can interact with any other unit in the PFD. For instance, adsorber A-1 can interact with adsorber A-2 for pressure equalization through the product-ends (v3) or the feed-ends (v4). Adsorber A-1 can also interact with any of the tanks in the PFD. If

A-1 is undergoing an elementary step where the flow is in the positive direction, these interactions happen through v1 and v2. Conversely, when the flow is in the negative direction, these interactions happen through v5 and v6.

In figure 4.2, the configuration of the PSA system cycle is illustrated, which consists of 6 steps with their respective durations and process flow paths. The steps are:

- Pressurization;
- Adsorption;
- Blowdown;
- Purge;
- Two steps of pressure equalization (step 3 and 6);

| | | | Step 1 | Step 2 | Step 3 | Step 4 | Step 5 | Step 6 |
|---|---|---|---|---|---|---|---|---|
| Duration | Value | seconds | 40 | 30 | 180 | 40 | 30 | 180 |
| Event | Value | - | None | None | None | None | None | None |
| | Unit | - | None | None | None | None | None | None |
| | Location | - | None | None | None | None | None | None |
| Adsorber 1 | Type | - | varying_pressure | varying_pressure | constant_pressure | varying_pressure | varying_pressure | constant_pressure |
| | Step Name | - | EQ-XXX-APR | RP-FEE-XXX | HP-FEE-RAF | EQ-XXX-APR | DP-ATM-XXX | LP-ATM-RAF |
| | Flow Direction | - | TBD | 0_(positive) | 0_(positive) | TBD | 1_(negative) | 1_(negative) |
| | Feed-end Valve | From | None | Feed_Tank_(T-1) | Feed_Tank_(T-1) | None | Valve_6_(v6) | Valve_6_(v6) |
| | | To | None | Valve_2_(v2) | Valve_2_(v2) | None | Atmosphere_(V-2) | Atmosphere_(V-2) |
| | | Type | Closed | Linear_Valve | Linear_Valve | Closed | Linear_Valve | onstant_Pressure_Controlle |
| | | Cv | 0.00E+00 | 2.31E-06 | 6.27E-06 | 0.00E+00 | 6.31E-06 | 1.00E+00 |
| | Product-end Valve | From | Valve_3_(v3) | None | Valve_1_(v1) | Valve_3_(v3) | None | Raffinate_Tank_(T-2) |
| | | To | Valve_3_(v3) | None | Raffinate_Tank_(T-2) | Valve_3_(v3) | None | Valve_5_(v5) |
| | | Type | Linear_Valve | Closed | onstant_Pressure_Controlle | Linear_Valve | Closed | Linear_Valve |
| | | Cv | 3.11E-06 | 0.00E+00 | 1.00E+00 | 3.11E-06 | 0.00E+00 | 1.15E-07 |
| Adsorber 2 | Type | - | varying_pressure | varying_pressure | constant_pressure | varying_pressure | varying_pressure | constant_pressure |
| | Step Name | - | EQ-XXX-APR | DP-ATM-XXX | LP-ATM-RAF | EQ-XXX-APR | RP-FEE-XXX | HP-FEE-RAF |
| | Flow Direction | - | TBD | 1_(negative) | 1_(negative) | TBD | 0_(positive) | 0_(positive) |
| | Feed-end Valve | From | None | Valve_6_(v6) | Valve_6_(v6) | None | Feed_Tank_(T-1) | Feed_Tank_(T-1) |
| | | To | None | Atmosphere_(V-2) | Atmosphere_(V-2) | None | Valve_2_(v2) | Valve_2_(v2) |
| | | Type | Closed | Linear_Valve | onstant_Pressure_Controlle | Closed | Linear_Valve | Linear_Valve |
| | | Cv | 0.00E+00 | 6.31E-06 | 1.00E+00 | 0.00E+00 | 2.31E-06 | 6.27E-06 |
| | Product-end Valve | From | Valve_3_(v3) | None | Raffinate_Tank_(T-2) | Valve_3_(v3) | None | Valve_1_(v1) |
| | | To | Valve_3_(v3) | None | Valve_5_(v5) | Valve_3_(v3) | None | Raffinate_Tank_(T-2) |
| | | Type | Linear_Valve | Closed | Linear_Valve | Linear_Valve | Closed | onstant_Pressure_Controlle |
| | | Cv | 3.11E-06 | 0.00E+00 | 1.15E-07 | 3.11E-06 | 0.00E+00 | 1.00E+00 |

*Figure 4.2 – Cycle configuration*

## 4.1.1 Input specifications

In order to perform a PSA simulation, the input conditions are varied according to the case study considered thanks to the Excel spreadsheets linked with the MATLAB code. This approach allow to evaluate the corresponding outputs and assess the system's performance under different scenarios. Since the feed binary stream is biogas with 60% of CH4 and 40% of CO2, the adsorbate properties has to be changed like the composition of the gas and its properties. Regarding the figure, in the description column reference is made to a *light key* which is the non-preferentially adsorbing species.

| Variable | Value | Unit | Comparisons | Variable Typ | Description |
|---|---|---|---|---|---|
| nComs | 2 | - | system property | scalar | The total number of components to be modeled in the system |
| nLKs | 1 | | system property | scalar | The number of light key components to be modeled in the system; the number of heavy key components are the total number of components minus the number of light key components. |
| sCom1 | CH4 | - | adsorbate properties | string | The chemical formula of the 1st component in a given system: ***define the 1st component to be the light*** |
| sCom2 | CO2 | - | adsorbate properties | string | The chemical formula of the 1st component in a given system: ***define the 1st component to be the light*** |
| molecWtC1 | 16 | g/mol | adsorbate properties | scalar | The molecular weight of the species i |
| molecWtC2 | 44 | g/mol | adsorbate properties | scalar | The molecular weight of the species i |

*Figure 4.3 – Adsorbate properties*

The input feed stream properties are presented in the following table, where yFeC1and yFeC2 are related to the fractional composition of $CH_4$ and $CO_2$ respectivaly:

| Variable | Value | Unit | Comparisons | Variable Typ | Description |
|---|---|---|---|---|---|
| tempFeed | 293.15 | K | system property | scalar | The fixed temperature of the feed stream coming into the feed tank, after being compressed and passing through the heat exchanger. |
| yFeC1 | 0.6 | - | adsorbate properties | scalar | The fixed feed mole fraction of ith component at a high pressure; the first component is the light key. |
| yFeC2 | 0.4 | - | adsorbate properties | scalar | The fixed feed mole fraction of ith component at a high pressure; the first component is the light key. |
| densFeGas | 0.00112 | g/cm3 | feed stream | scalar | Gas density of the feed gas mixture. |
| viscFeGas | 0.0000133 | Pa-sec | feed stream | scalar | Viscosity of the feed gas mixture. |

*Figure 4.4 – Feed stream properties*

The material used in the simulation as adsorbent is Zeolite 5A. Among the all features of adsorbent properties, the most relevant regard the LDF mass transfer coefficient that governs the adsorption kinetics for each component. The values used are 0.049 and 0.021 for $CH_4$ and $CO_2$, in zeolite 5A, respectively [44].

| Variable | Value | Unit | Comparisons | Variable Typ | Description |
|---|---|---|---|---|---|
| ldfMtc1 | 0.049 | 1/sec | physical properties | scalar | The linear driving force mass transfer coefficient for ith component; the first component is light key |
| ldfMtc2 | 0.021 | 1/sec | physical properties | scalar | The linear driving force mass transfer coefficient for ith component; the first component is light key |

*Figure 4.4 – Adsorbent Properties*

The physical properties of the adsorbent, zeolite 5A, are shown in Table 4.1 and all properties of the column are described in Table 4.2

| Adsorbent property | Zeolite 5A |
|---|---|
| Pellet density (kg/$cm^3$) | 0.00166 |
| Bulk density (kg/$cm^3$) | 0.00795 |
| Pellet diameter (cm) | 0.314 |
| Adsorbent mass (kg) | 1.2 |

*Table 4.1 – Physical properties of Zeolite 5A*

| | |
|---|---|
| Column length (cm) | 100 |
| Column inner radius (cm) | 2.2 |
| Column outer radious (cm) | 2.55 |
| Bed porosity | 0.314 |
| Column density (kg/$cm^3$) | 0.00783 |

*Table 4.2 – Adsorber columns characteristics*

### 4.1.2 Output simulation

This section analyzes the effect of the adsorption pressure, desorption pressure and adsorption time of the simulated PSA cycles. The key indicators of the cyclic performance, $CO_2$ and $CH_4$ purity and recovery, are estimated once the cyclic steady-state is achieved. The reference case is the basis to run the sensitivity analysis by changing one parameter at a time.

## EFFECT OF ADSORPTION PRESSURE

The influence of the adsorption pressure is assessed by varying it between 5 and 11 bar in different simulation cases. The duration of the pressurization and depressurization steps are assumed constant in all the simulations. At higher adsorption pressure the $CH_4$ purity reaches a maximum due to the enhanced adsorption of $CO_2$; conversely the recovery of methane drops down linearly with the adsorption pressure. As may be expected, the opposite trend is observed in the pattern of $CO_2$ purity and recovery.

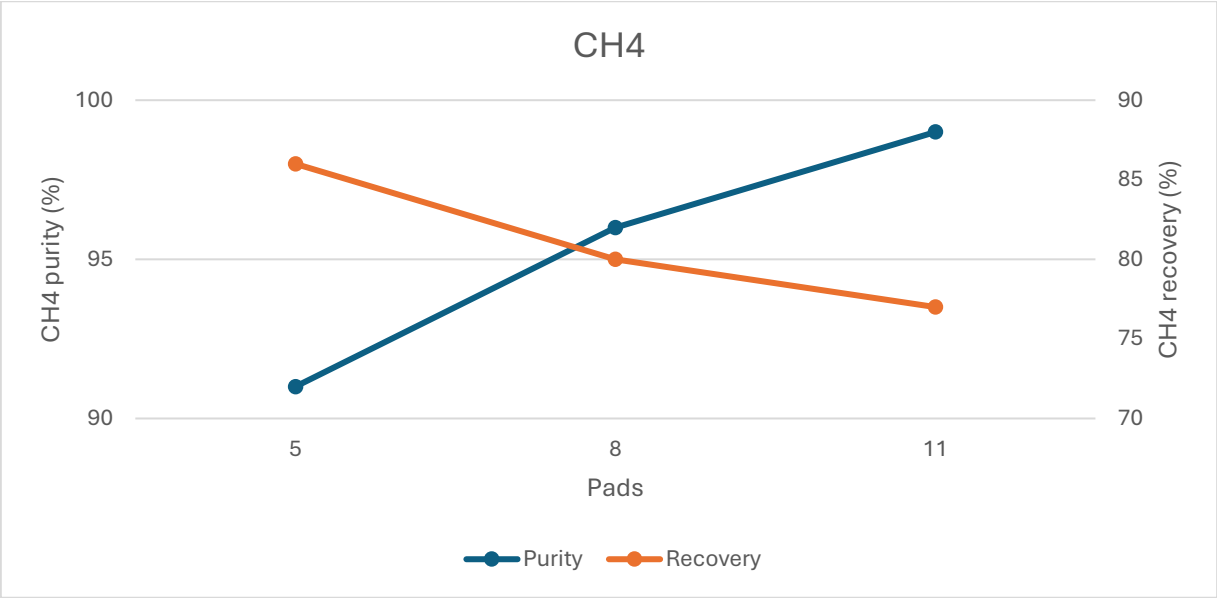


*Figure 4.5 – Effect on $CH_4$ purity and recovery*

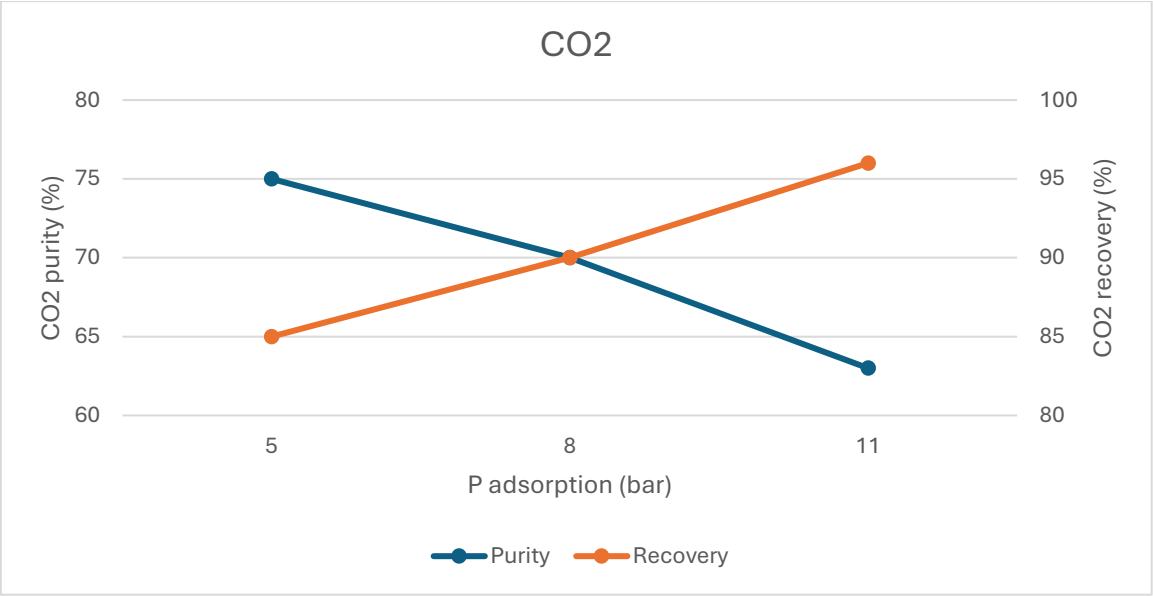


*Figure 4.6 – Effect on $CO_2$ purity and recovery*

At higher pressures, the zeolites, the adsorbent, adsorbs $CO_2$ more effectively and therefore preferentially. This results in a higher purity $CH_4$ stream in the product. While the $CH_4$ in the product is purer, it can also lead to a situation where some $CH_4$ is also adsorbed or lost in the purge stream at a higher adsorption pressure. The $CO_2$ selectivity of the adsorbent increases with increasing pressure, which may hinder the adsorption of $CH_4$ and thus reduce the recovery. Boosting the adsorption pressure implies that the feed gas is compressed to a higher level and, therefore, more energy is needed to reach and sustain pressures, which increase the overall compression energy consumption. At higher pressures, the adsorbent binds more $CO_2$ because of the higher interaction, and thus, more efficient separation and recovery of $CO_2$ is possible during the desorption stage.

## EFFECT OF DESORPTION PRESSURE

Different pressures between 0.5 bar and 1.0132 bar were set during the regeneration stage to assess the influence of the desorption pressure on the process performance parameters. As may be expected, $CO_2$ recovery increases when the pressure is low. It is because of better regeneration of the adsorbent under these conditions. However, it should be recalled that the higher the vacuum level, the more the energy demand of the system. Concerning $CH_4$, a lower pressure during the blowdown step results purity in the product stream. A lower pressure enhances the regeneration of the bed and substantially reduces the presence of $CO_2$ in the product stream.

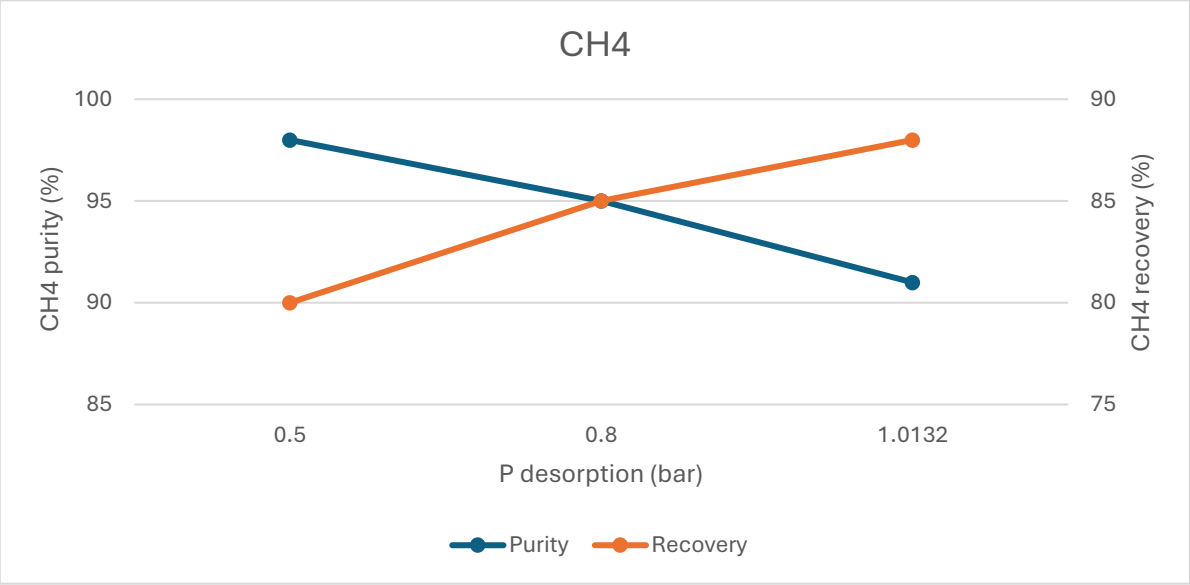


*Figure 4.7 – Effect on CH4 purity and recovery*

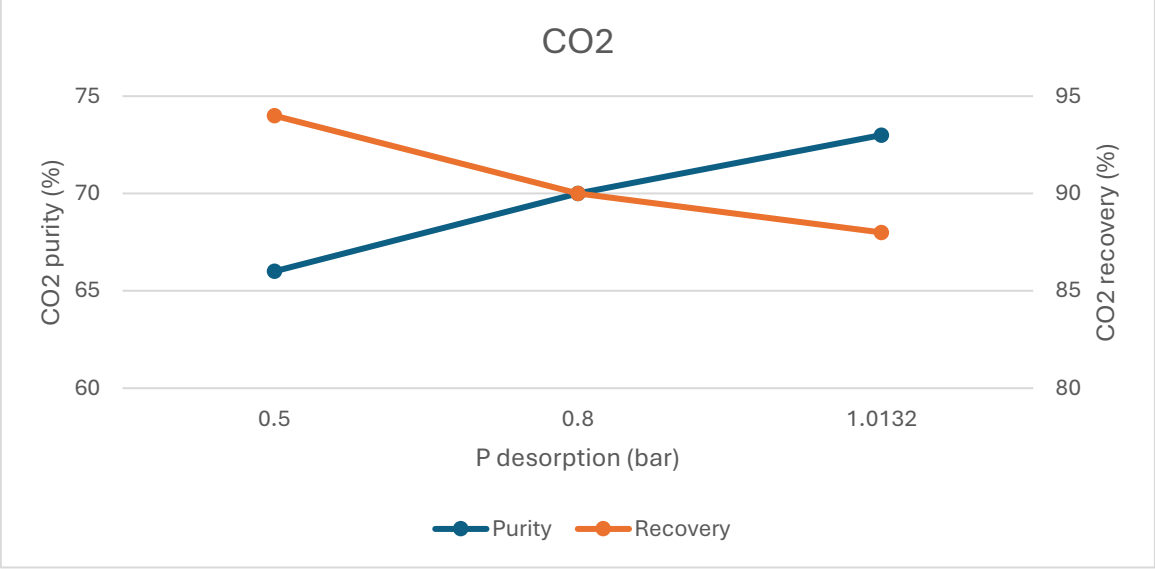


*Figure 4.8 - Effect on $CO_2$ purity and recovery*

In the PSA process, the cycle is based on a high-pressure adsorption phase and a low-pressure desorption (or regeneration) phase. When the desorption pressure is increased, the degree of vacuum applied during regeneration is reduced. With a higher desorption pressure, the adsorbent is not completely emptied of the adsorbed species. In particular, residual $CO_2$ ,or other contaminants, remains in the bed and can co-desorb with $CH_4$, leading to a reduction in the methane purity of the product stream. A less profound desorption means that less $CH_4$ is lost in the regeneration flow. Thus, although the purity is lower, a larger fraction of $CH_4$ is recovered because the gas that would otherwise be pushed out is retained in the adsorption cycle. Higher desorption pressure also promotes the desorption of $CO_2$. As a result, the amount of $CO_2$ recovered, removed from the adsorbent bed increases because the attractive forces are not counteracted by such a deep vacuum. An increase in the desorption pressure implies that the system must work to maintain higher pressures during the regeneration cycle. This translates into a greater energy requirement, for example, for compressors or pumps, compared to a configuration operating at lower desorption pressures.

## INFLUENCE OF ADSORPTION TIME

In a PSA process, the adsorption time must be carefully balanced. If the adsorption period is too short, not the entire bed is utilized, which reduces the separation capacity. On the other hand, if the adsorption time is too long, the bed becomes saturated, and $CO_2$ breaks through into the product gas, lowering the recovery. Thus, in order to find the optimal time, it is been varied between 180 and 540 seconds , although the timing of the other steps remained. By extending the adsorption time, the adsorbent bed quickly approaches the saturation point for the $CO_2$. Once the adsorbent can no longer retain all the $CO_2$, it begins to mix with the produced $CH_4$, lowering its purity. A longer adsorption time allows a larger volume of incoming gas to be processed. As a result, although some $CH_4$ is accompanied by $CO_2$ during the phase, a greater fraction of $CH_4$ is recovered overall because the cycle handles a higher flow before regeneration. Therefore, although purity decreases, productivity is increased. With the extended adsorption time, $CO_2$ begins to break through earlier than expected, being carried away with the product stream instead of staying adsorbed and later recovered during the regeneration phase. In other words, some of the $CO_2$ escapes the adsorption process, reducing the fraction of $CO_2$ actually recovered afterward.

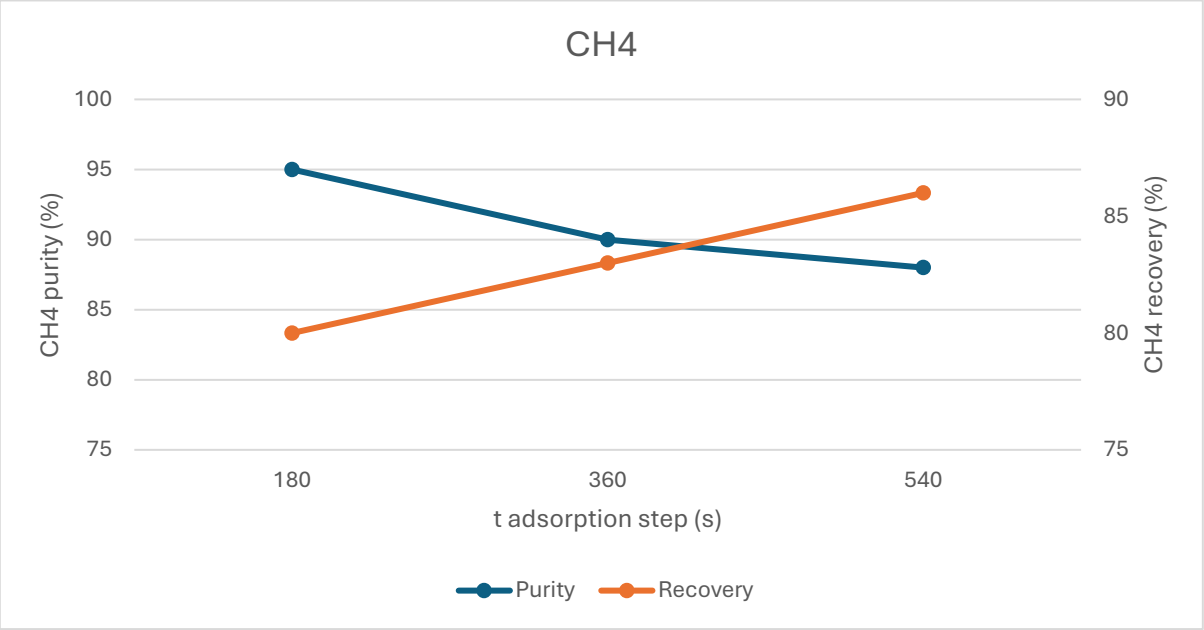


*Figure 4.5 – Effect on CH4 purity and recovery*

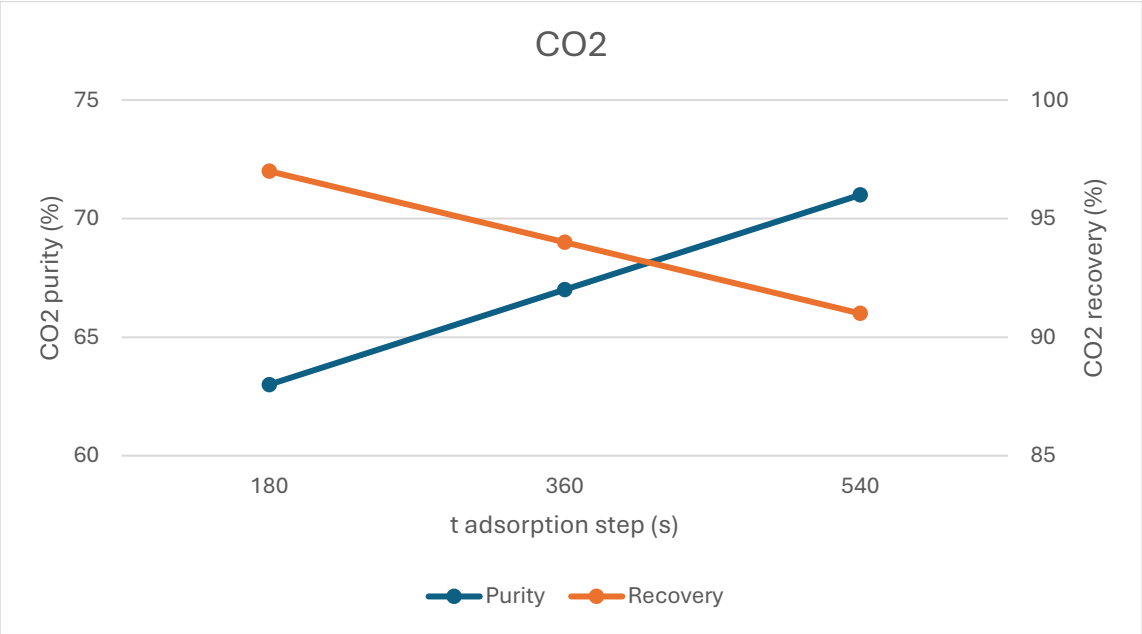


*Figure 4.6 – Effect on CO2 purity and recovery*

## 4.2 Electrolyzer Model

In this section, a study is conducted using the Ulleberg model illustrated in the section 3.1, to investigate the effect of operating temperature, pressure and current density on the performance of the cell stack. Before moving on to the Aspen Plus for the alkaline electrolyzer model, the starting point is the sizing the electrolyzer using the mathematical model. The following graphs illustrate various operating points in order to identify an optimal working condition. In these graphs, key performance metrics are plotted against operating parameters such as current density, cell voltage, and operating temperature and pressure. The Ulleberg model provided us with a framework to predict the behaviour of the electrolyzer under different conditions. But in this case, the constraint that has to be respected is the hydrogen moles produced by the electrolyzers that has to be 4 times the $CO_2$ moles captured by the PSA system for methane production. So in order to respect this condition, the variable is the number of cells considered in the stack. The stack power has been calculated with the following equation:

$$P_{stack} = V_{cell} \cdot N \cdot I \tag{29}$$

where $V_{cell}$ is the voltage cell, N is the numbers of cells of stack and I is the current calculated as the product between the current density $i$ (A/$m^2$) and the active electrode area ($m^2$) assumed equal to 0.1.

These analyses allow to define an optimal set of operating conditions that balance efficiency, energy consumption, and operational stability. With these insights, we are now prepared to incorporate the chosen operating point into our detailed Aspen Plus model, ensuring that our simulation accurately reflects the real-world behaviour of the alkaline electrolyzer.

## INFLUENCE OF TEMPERATURE AND CURRENT DENSITY

Figure 4.11 and figure 4.12 shows the polarization curve and power required by the alkaline electrolysis stack at different temperatures. According to the model, when the temperature increases from 50°C to 90°C, the voltage progressively reduces . As a consequence, the stack power required in the electrolysis decreases when the temperature is higher. This is because, as the temperature increases, the Gibbs free energy required for electrolysis decreases, and the reaction kinetics are accelerated. Additionally, the conductivity of the electrolyte improves, lowering the ohmic overpotential, and thus the overall electrolysis voltage decreases.

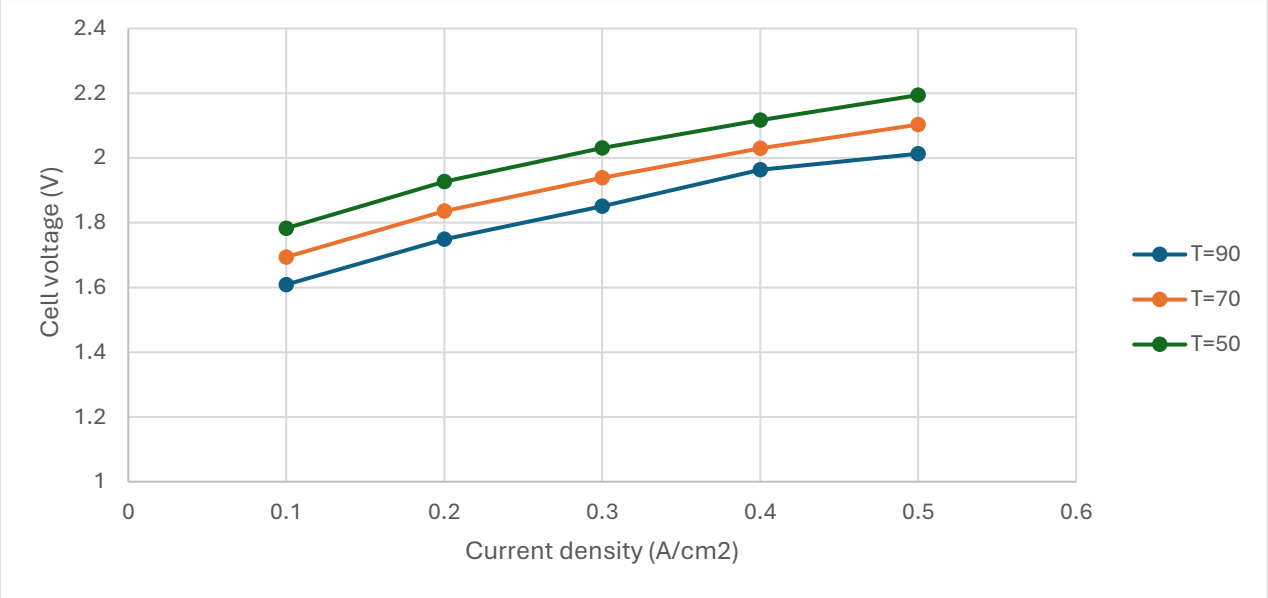


*Figure 4.7 – Effect of temperature on polarization curve at 7 bar*

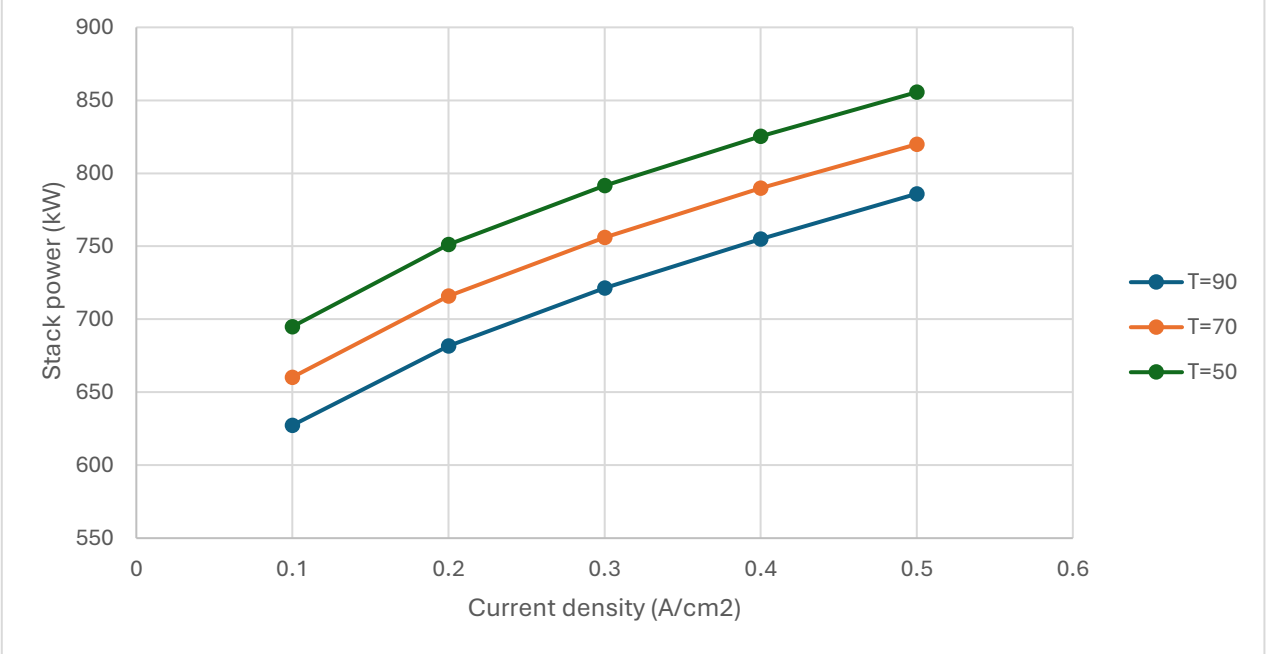


*Figure 4.12 – Effect of temperature on stack power at 7 bar*

## INFLUENCE OF PRESSURE AND CURRENT DENISTY

Figure 4.13 and figure 4.14 shows the polarization curve and power required by the alkaline electrolysis stack at different pressures but the effect of temperature on voltage is more significant than that of pressure. On the one hand, when the pressure raises the void fraction between electrodes is reduced due to smaller size of generated gas bubbles. This reduction in bubbles sizes also affects the effective contact area between electrodes and electrolyte, which results in lower ohmic resistance and required cell voltage. On the other hand, the reversible cell voltage increases with the pressure. As a consequence, in the pressure range studied, these phenomena are counter balanced and ohmic overpotentials increase slightly when the pressure increases.

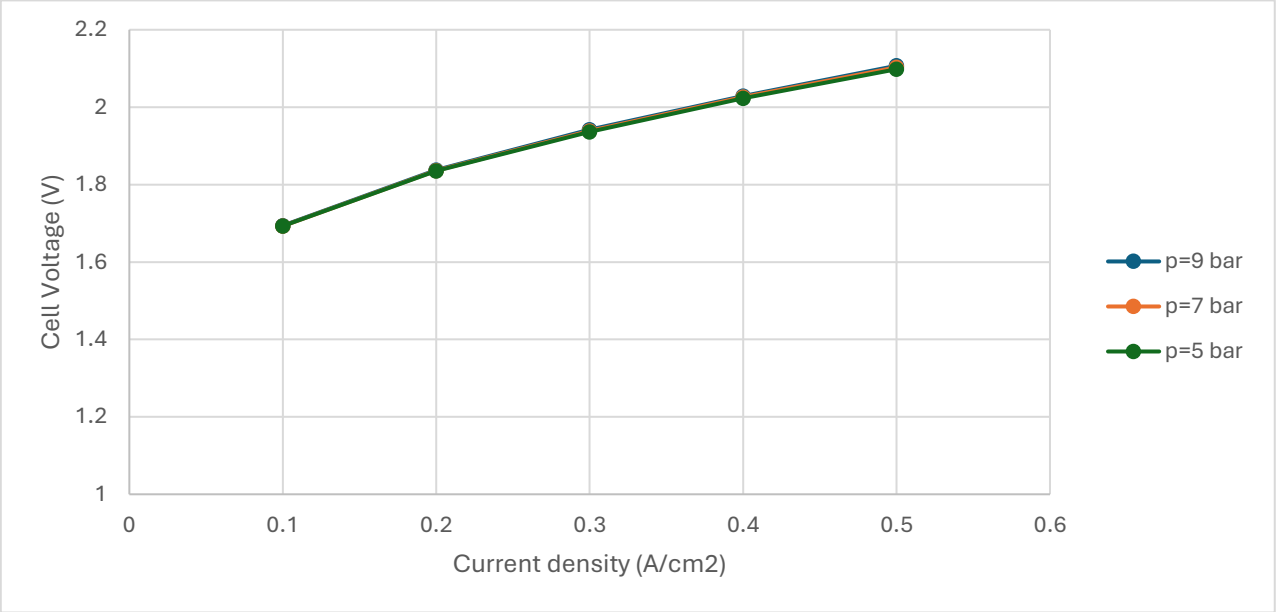


*Figure 4.13 – Effect of pressure on polarization curve at 70°C*

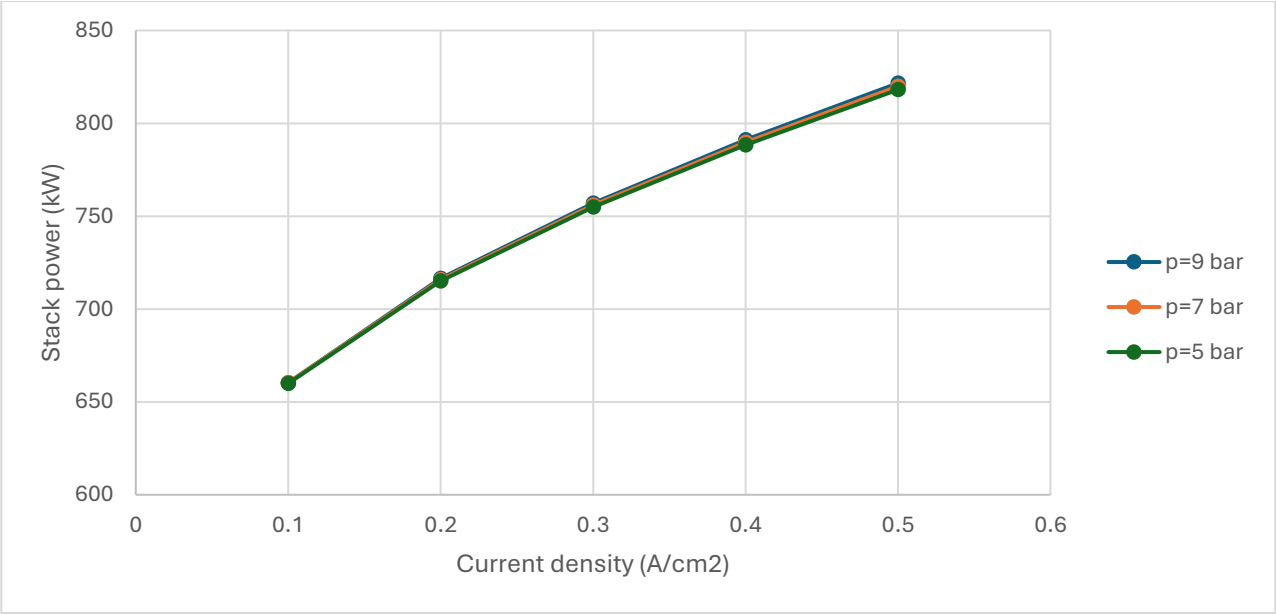


*Figure 4.14 – Effect of pressure on stack power curve at 70°C*

## EFFICIENCY EVALUATION

To assess the overall performance of the system, the stack efficiency should be calculated. The efficiency represents the ratio of the energy contained in the useful products of a process to the energy contained in all input streams. Therefore, the energy efficiency for hydrogen production from an electrolysis system is formulated as follows:

$$\eta_{sy} = \frac{n_{H2} \cdot LHV_{H2}}{W_{net}} \tag{30}$$

where $LHV_{H2}$ is the hydrogen lower heating value; $n_{H2}$ is the outlet flow rate of hydrogen in the electrolysis plant; $W_{net}$ is the electric power input to the AEL system. The electric power input is calculated as sum of the power stack, pump and heater.

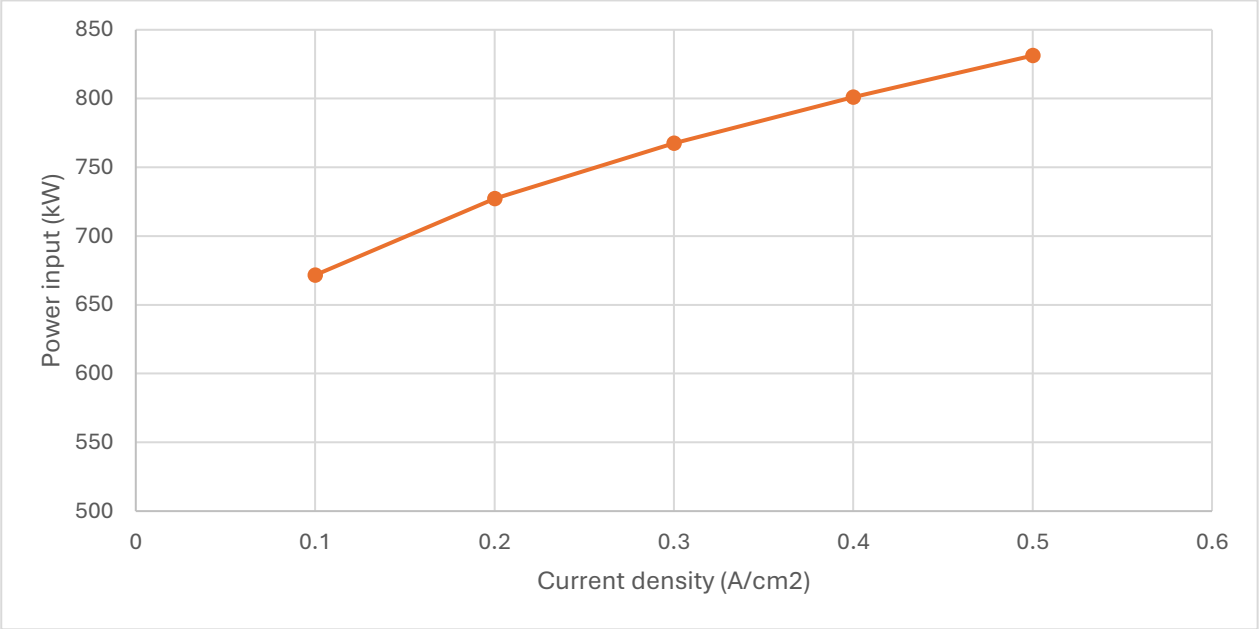


*Figure 4.15 – Stack power curve at 70°C and 7 bar*

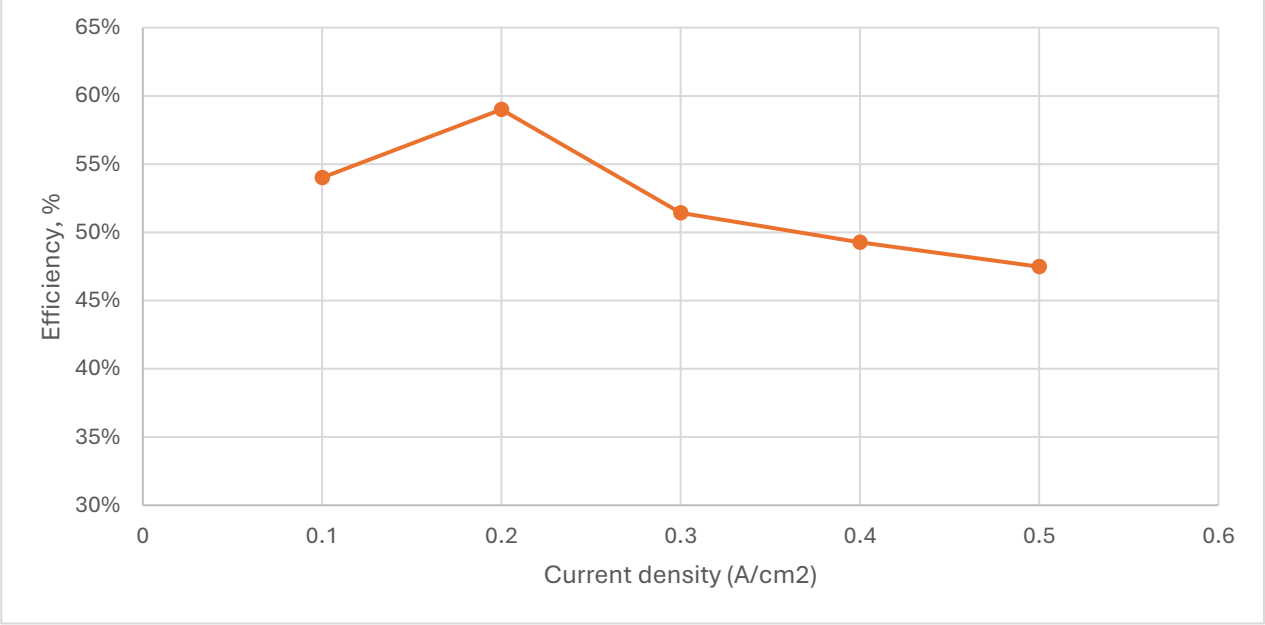


*Figure 4.16 – Efficiency curve at 70°C and 7 bar*

### 4.2.1 Electrolyzer Aspen model

After a sensitivity analysis for the parameters of electrolyzer, as input data in Aspen Plus software have been used referring the working point with maximum efficiency, which is 60%. The two streams of $CO_2$ and $H_2O$ enter in parallel.

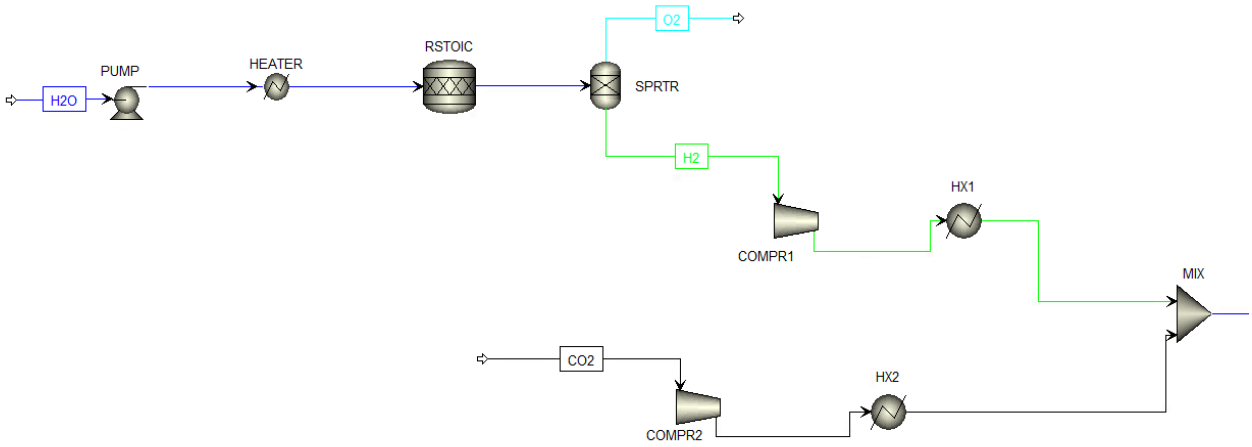


*Figure 4.17 – Flowsheet for CO2 and H2O*

The water, at 20°C and 1 bar, pass to PUMP and HEATER block where the pressure is increased. Then, is send to RSTOIC which is a stoichiometric reactor, used to simulate water electrolysis. This reactor requires the knowledge about reactant, products and fractional conversion. The following reaction will be put in the model:

$$H_2O \rightarrow H_2 + \frac{1}{2} O_2$$

This does not accurately represent what occurs in an electrolysis cell. However, since Aspen Plus cannot simulate an electrochemical device, this approach serves as the only viable method to model water electrolysis. No electrons are involved in the simulation, meaning that what would typically be an electrical input in a real system is instead represented as Heat Duty. This difference only affects the way energy is accounted for, without altering the numerical results. Additionally, the stoichiometric reactor requires defining the fractional conversion of a key reactant.

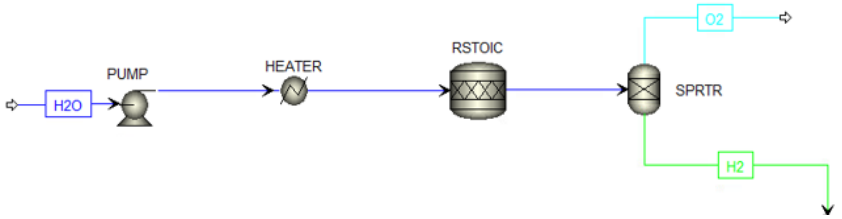


*Figure 4.18 – Alkaline eletrolyzer model*

SPRTR is a separator which realizes effectively the physical separation between anode and cathode side. After the water electrolysis, hydrogen is compressed, in parallel with carbon dioxide flow, at a pressure equal to 20 bar and mixed in MIX block flowing into the methanation section.

### 4.2.2 Methanation section

MET1, MET2 and MET3 are the three methanation reactors, simulated with a Gibbs Reactor, a reactor which takes a mixture to chemical equilibrium by minimizing Gibbs Energy. Reactors are simulated as adiabatic. Upstream of MET2, there is a block that permits a recycle in order to limit the temperature increase up to 700°C.

HM1, HM2, HM3 and HM4 are intermediate coolers which refrigerate the outlet mixture from the previous methanation reactor, in order to allow a subsequent equilibrium which will increase the fraction of methane in the mixture. HM1, HM2 and HM3 set outlet temperature to 220°C. HM4 cools mixture to 35°C.

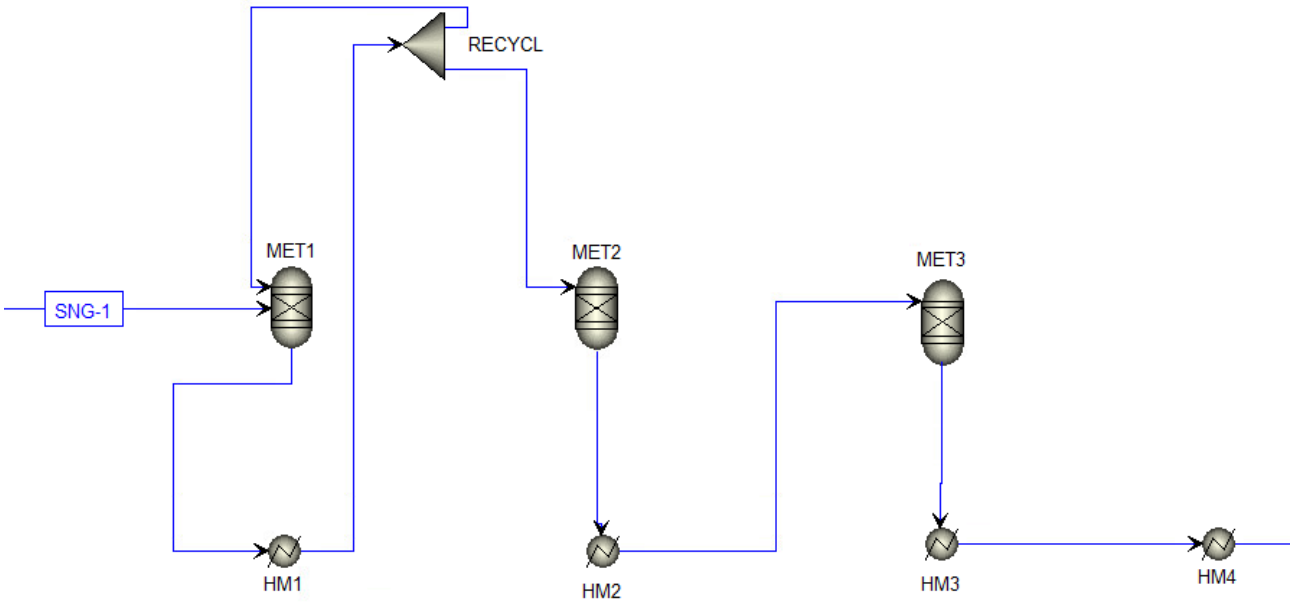


*Figure 4.19 – Methanation section on ASPEN PLUS*

### 4.2.3 Natural gas correction

DRUM is a Flash separator which allows thermodynamic equilibrium between liquid phase and gaseous phase. This component allows separating from the gas a huge fraction of water, which is a product of both methanation reactions and is present in high concentration.

SIEVE is a molecular sieve which retains substances as water and carbon dioxide. It has been considered that molecular sieve retains almost all the water and 98.5% of carbon dioxide [45].

SNGC1, SNGC2 and SNGINTC are components of natural gas compression section, bringing gas pressure to a value of 60 bar, which is a typical value of natural gas pipelines pressure.

N2COMP1, N2COMP2 and N2INTC are components of nitrogen compression section. Indeed it has been verified that SNG produced doesn't respect prescriptions established by authorities. In this case

prescriptions established in Italy (by "Snam Rete Gas") for pumping natural gas into pipelines have been used [46].

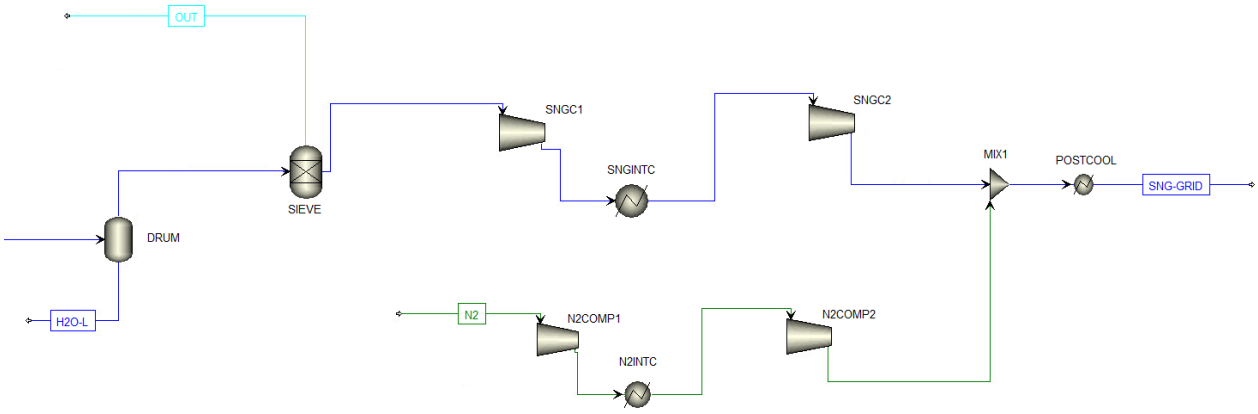


*Figure 4.19 – Correction section on ASPEN PLUS*

In order for the gas to be introduced into the national network, it must respect certain parameters. For this thesis work, prescriptions established by Snam for pumping natural gas into pipelines are used [46]. The main constraints regard three parameters:

- Gas Gravity;
- Wobbe Index;
- Higher Heating Value of produced SNG.

Gas Gravity is the ratio between densities of produced SNG and air, both calculated at "Standard conditions", i.e. 101.325 Pa and 288,15 K (according to [46] and ISO 13443).

$$GG = \frac{\rho_{SNG}}{\rho_{air}} \tag{31}$$

Where $\rho_{air}$ is set to 1,22 kg/$Sm^3$ assuming a mole mass of 28,84 kg/kmol.

Wobbe Index is expressed by the following equation:

$$WI = \frac{HHV}{\sqrt{GG}} \tag{32}$$

HHV is the Higher Heating Value of SNG.

Note that, during evaluation of HHV related to pipeline prescriptions, only methane (and not hydrogen) contribution was prudently considered, despite also hydrogen is a fuel.

Acceptability boundaries for these parameters are summarized in following table:

| | |
|---|---|
| HHV [MJ/$Sm^3$] | 34.95 – 45.28 |
| Wobbe Index [MJ/$Sm^3$] | 47.31 – 52.33 |
| GG | 0.5548-0.8 |

*Table 2 – Boundaries accepted by the SNAM (Italy) grid*

The produced SNG has too low density, and consequently too low Gas Gravity. Being the SNG mostly composed by light molecules such as hydrogen and methane, it is too light. So, it is necessary to "correct" SNG with a diluent. Nitrogen is chosen, and the target value of GG is set to 0,555.

After the methanation and the cleaning section, a SNG with the following composition is obtained:

| Component | |
|---|---|
| $CH_4$ | 95,3% |
| $H_2$ | 1.8% |
| $N_2$ | 2.8% |

*Table 4.3 – SNG final composition*

## 4.3 Plant efficiency

The efficiency of the plant is calculated as the ratio between Chemical Power associated to SNG and the total electric power in input (A.C.).

The electrical input is made of several contribution :

- Electrical input in AC for the stack (electrolysis cells operate in DC);
- Electricity to run pumps and compressors;
- Electricity for external heat requirements.

So, efficiency can be calculated as follows:

$$\eta_{sy} = \frac{POWER_{SNG}}{W_{el}} = \frac{m_{SNG} \cdot LHV_{SNG}}{W_{el}} \tag{33}$$

LHV is calculated considering the final molar composition of SNG, after the correction section (both methane and hydrogen are considered as fuels). For the electricity to drive pumps and compressors both isentropic and electric efficiency are considered, their values are:

| | |
|---|---|
| LHV methane, MJ/kg | 50 |
| LHV hydrogen, MJ/kg | 120 |
| $\eta_{is,COMPR}$ | 0,75 |
| $\eta_{is,PUMP}$ | 0,80 |

| | |
|---|---|
| $\eta_{AC/DC}$ | 0,98 |

*Table 3.4 - Hypothesis*

Bringing to the following results:

| | |
|---|---|
| $W_{in,AWE}$ [kW] | 715 |
| $W_{COMPR,H2}$ [kW] | 10 |
| $W_{COMPR,CO2}$ [kW] | 4 |
| $W_{COMPR,SNG}$ | 3 |
| $W_{COMPR,N2}$ [kW] | 3,2 |
| $W_{PUMP}$ [kW] | 1,07 |
| $W_{PRE-HEAT}$ [kW] | 2,11 |
| $W_{EXT-HEAT}$ [kW] | 290 |
| $W_{EL-TOT}$ [kW] | 1028.3 |
| $LHV_{SNG}$ [MJ/kg] | 47,9 |
| $mass\ flow\ rate\ _{SNG}$ [kg/s] | 0,0095 |
| $Chemical\ Power_{SNG}$ [kW] | 455 |
| EFFICIENCY | 44,2 % |

*Table 4.4 – Plant results*

## 4.4 Economic analysis

The economic evaluation carried out in this work is based on the concept of Net Present Cost (NPC), that is, the identification of the all costs related to a plant for the entire period of its life that are expressed in the present value [47]. This data is the very useful for the comparison between different plants and technologies.

$$NPC = CAPEX_0 + \sum_{J=1}^{n} [\frac{OPEX_j}{(1+d)^j} + \frac{RC_j}{(1+d)^j}] \quad (34)$$

Where:

- $n=20$ is the analysis period, in years;
- d is the corrected discount rate (considering an expected inflation rate);
- $CAPEX_0$ represents the capital expenditures due to the investments done at the beginning of the analysis period;
- $OPEX_j$ represents the cost of the operational phase in the j-th year. It accounts for the maintenance of the plant as well as all the expenditures necessary during the year;
- $RC_j$ accounts for the replacement cost as periodically it is necessary a periodic substitution of components to maintain reliable the operation of the system.

The discount rate variable, d, extends the economic analysis to the entire life of the plant and it can be calculated through an economic formulation used in reference. In this way it is possible to determine any future cost at the present value:

$$d = \frac{d' - ir}{1 + ir} \quad (35)$$

Where:

- $d'$ is the nominal discount rate, assumed equal to 7% [47];
- $ir$ corresponds to inflation rate, equal to 2% [47].

Such that the real discount rate is 5%.
Another hypothesis that has to be fixed is the capacity factor of the plant, defined as the ratio between the operating hours of the system and the total yearly hours:

$$CF = \frac{working\ hours}{8760} \quad (36)$$

For the analysis, a CF equal to 90% is fixed, so the total working hours of the plant are 7884. This ratio is important for assessing the total production of SNG as well as the consumption of fuels and the frequency of substitutions.

### 4.4.1 Capex plant

The capital expenditures are composed by the investment costs for the electrolysis part that includes the cost of the alkaline stack, auxiliaries equipment and plant preparation cost. On the other hand, the methanation section considers the cost function the power of the SNG obtained at the end of the process including transport, installation and commissioning.

For the AWE section there is:

- Stack cost assumed 1500 €/$kW_e$ including balance of plant, transport, installation and commissioning from ENEA [48] ;

For the methanation part there is:

- Cost assumed 600 €/$kW_{SNG}$ with the reference to HHV [49] ;

### 4.4.2 Opex plant

In the Operating Expenditure are included all the cost for activities that occur once the system starts to operate. In particular, the following expenditures are considered:

- Electrolyzer Operation and maintenance costs: the general maintenance cost is fixed from 4-5% of the total CAPEX per year [48], reaching a value of 53625€ ;
- Replacement stack cost: the stack replacement is fixed to the 30% of the total investment cost and the substitution is performed every 6 years [48] with a cost of 321750€;
- Methanation Operation and maintenance costs: maintenance cost is fixed at 10% of the total CAPEX per year [49], reaching a value of 100915,2€. This value includes also include costs for catalyst replacement;
- Labour cost: 120.000 € per year obtained for 4 workers.
- The expenditure relating to electricity depend on plant utilization. Electricity is used to run both AWE and methanation sections, and its cost is fixed to 50 €/MWh. For the electrolyzer and the methanation, the electricity cost is 281853€ and 179361€ respectively.

Since a $CO_2$ capture process using PSA is under consideration, an additional cost to take into account is the installation and operating cost of the system capture from biogas upgrading. Then, the difference in the levelized cost of methane will be compared, both without and with the capture system. For the PSA system, the following costs are taken into account, for a biomethane production of 100 $m^3/h$ [50]:

- The investment costs accounts for 10400€/($m^3/h$);
- The operational costs are 12.8 $c$€/($m^3/h$).

### 4.4.3 Results

The aim of this section is to consider and quantify in economic terms the fruits of the sizing and operations carried out by the P2G plant. According to (34), the following values are respectively for the case in carbon dioxide free source and the other in case of PSA carbon capture:

| | $CO_2$ FREE SOURCE | $CO_2$ PSA SOURCE |
|---|---|---|
| TOTAL NPC, M€ | 10.08 | 12.33 |

*Table 4.5 – NPC values*

Starting from NPC, it is possible to calculate other variables to provide even more accurate indications from the point of view of convenience of the plant. To quantify the SNG produced in monetary terms, another cost value can be considered as a function of the energy contained, to be able to compare it with the other variables. The following equation therefore allows to estimate the cost at which 1 MWh produced by the SNG should be sold [47]:

$$LCOM = \frac{NPC}{\sum_{J=1}^{n} \frac{SNG\ produced_J}{(1+d)^j}} \tag{37}$$

The results are:

| | $CO_2$ FREE SOURCE | $CO_2$ PSA SOURCE |
|---|---|---|
| LCOM, $€/MWh$ | 236.9 | 289.7 |
| LCOM, €/ $kg_{CH4}$ | 3.15 | 3.85 |

*Table 4.6 – LCOM values*

In case of the presence of the carbon capture system, the values both of NPC and LCOM is higher than the other case due to the cost of PSA system and its operation.

In following picture the weight of each kind of cost is shown for both cases:

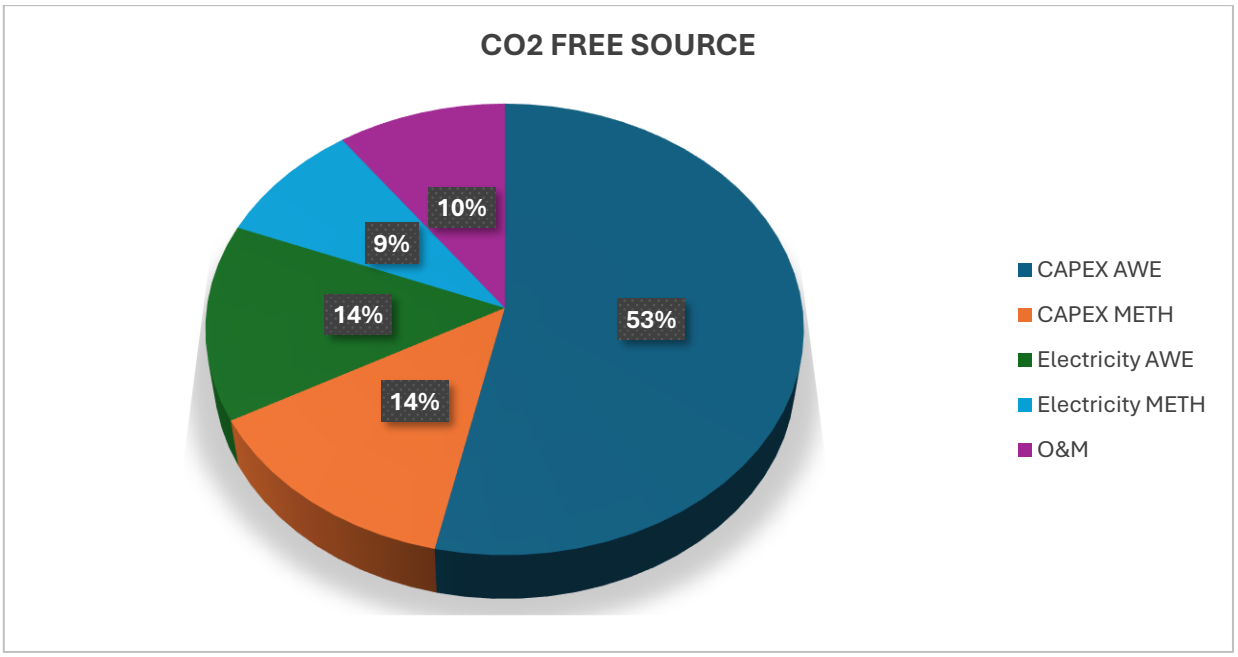


*Figure 4.20 – Total plant costs breakdown*

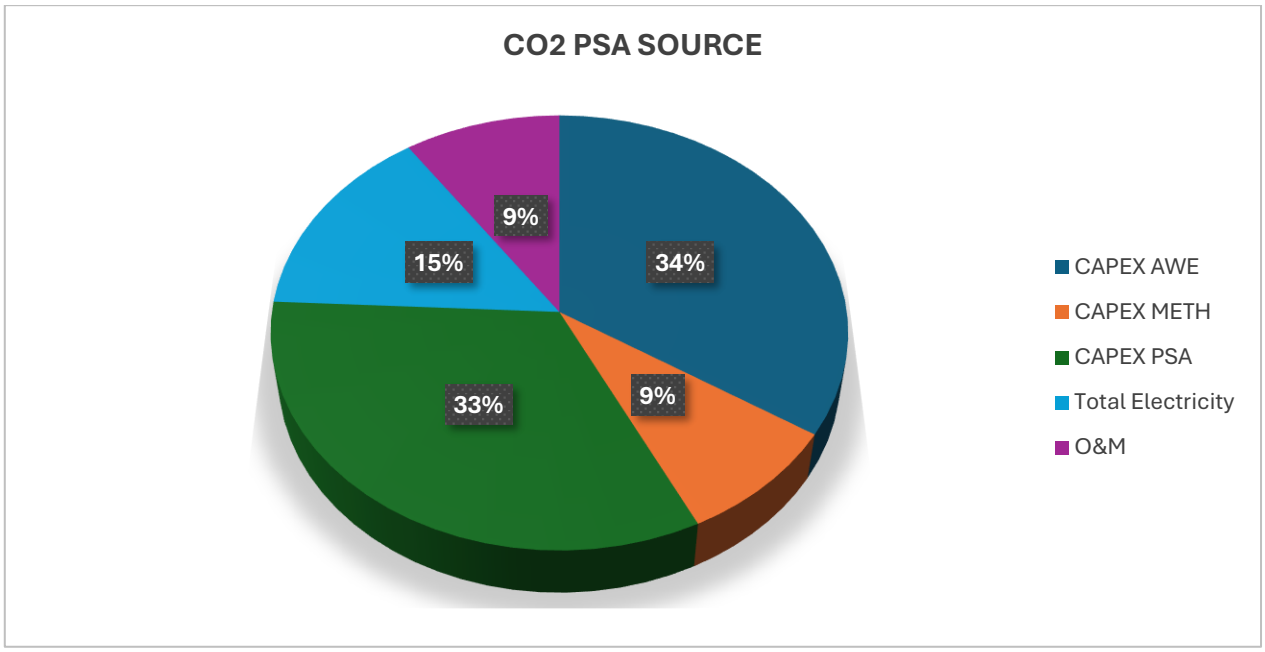


*Figure 4.21 – Total plant costs breakdown*

As can be seen from the previous figures, it is evident that in the base case, where the capture system is not considered, the highest cost is that of the electrolyzer section. However, when the capture system is considered, the investment costs of PSA system and electrolyzer are of the same order of magnitude, followed by the electricity consumption.

### 4.4.4 Sensitivity analysis

The following figures, describes for both cases, the variation of costs in function of the electricity price, considering a range from 0 to 200 $€/MWh$. The breakeven point is almost reached only if the electricity cost consumed is nearly zero in case of household natural gas. As expected, the behaviour of LCOM is linearly dependent from the electricity price.

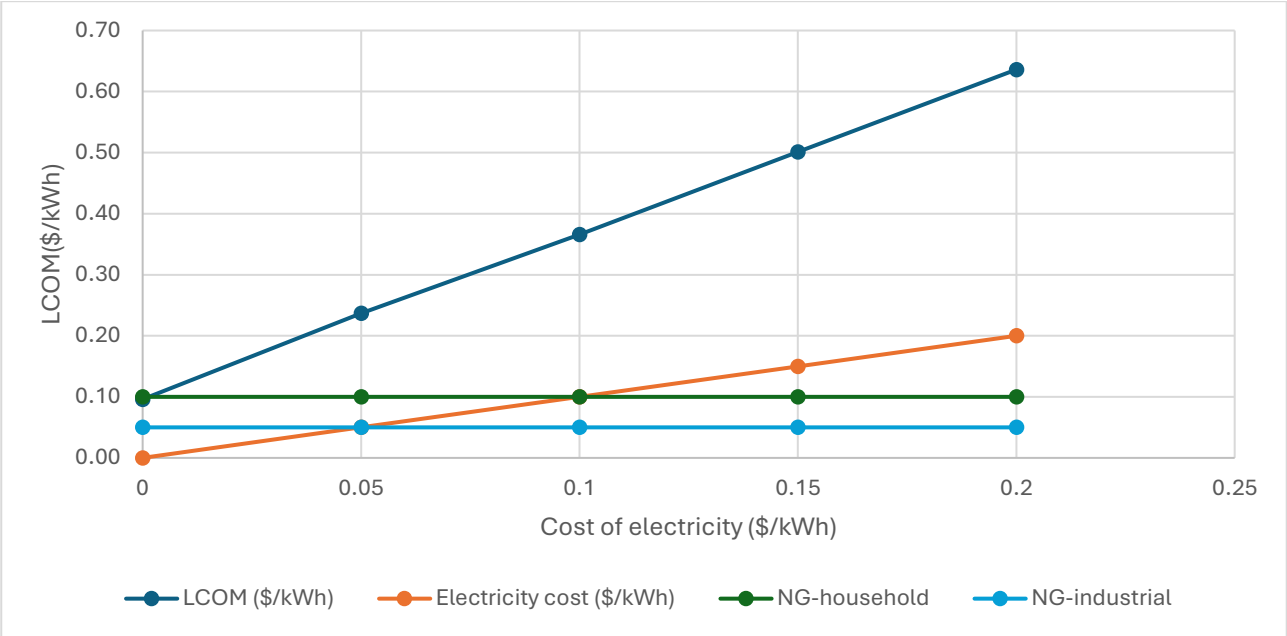


*Figure 4.22 – Varying cost of electricity without capture system*

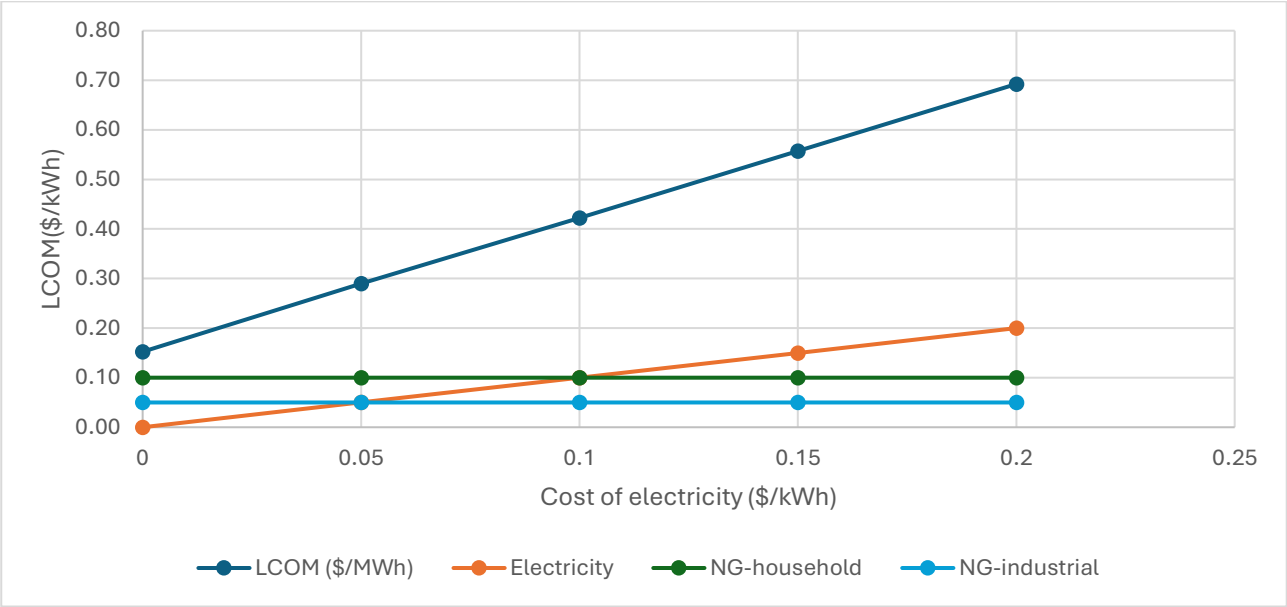


*Figure 4.23 – Varying cost of electricity with capture system*

## CONCLUSIONS

In this work, a plant for SNG production from biogas through carbon dioxide capture, water electrolysis and methanation has been analyzed.

In the capture process, a PSA system was used and its operating conditions were set by varying the main operating parameters to evaluate the performance metrics with focus on purity and recovery of $CO_2$ and $CH_4$. First, on $CO_2$, it was seen that at different pressures in the adsorption and regeneration modes, a maximum purity of about 75% can be obtained with a high recovery but with some $CH_4$ present.

The alkaline electrolyzer was simulated using the Ulleberg model which includes the thermodynamic and electrochemical modeling. Some operating conditions were considered and evaluated as a function of pressure and temperature since $H_2$ and $CO_2$ have a stoichiometric relationship and the optimum condition was chosen to obtain a maximum efficiency of 60%. After modeling the electrolyzer and the methanation section in Aspen Plus, the quality of the produced SNG was evaluated.

An economic analysis of the integrated plant of PSA, alkaline electrolysis and methanation was carried out. Key performance indicators, such as the net present cost and the levelized cost of methane, were estimated. The LCOM in the systems investigated with and without the $CO_2$ capture system is 3.15 €/kg $CH_4$ and 3.85 €/kg $CH_4$, respectively. In the case without the capture system, the main cost is the electrolyzer stack, and in the other case the main costs are the investments in the PSA system and the electrolyzer. This comparison shows the economic competitiveness of the synthetic methane produced versus other power-to-gas pathways.

At the end, based on the above methodology, the economic analysis did not incorporate any form of revenue or incentives which would represent a significant source of income and therefore, this technology could be competitive.

# References

[1] G. R. H. R. P. Rafael M.Siqueira, “Carbon dioxide capture by pressure swing adsorption,” 2017.

[2] IEA, “CO2 Emissions,” IEA, 2021.

[3] IEA, “Energy Technology Perspectives,” 2020.

[4] L. J. O. R. F. D. T. R. Tapia J.F.D., “A review of optimization and decision-making models for the planning of,” *Sustainable Production and Consumption,* 2017.

[5] M. A. W. Seyed Ehsan Hosseini, “Hydrogen production from renewable and sustainable energy resources: Promising green energy carrier for clean development,” *Renewable and Sustainable Energy Reviews,* 2015.

[6] W. K. W. L. J. L. P. Z. R. B. A. S. a. T. E. M. Peter Markewitz, “Worldwide innovations in the development of carbon capture technologies and the utilization of CO2,” *Energy & Environmental Science,* 2012.

[7] R. L. D. A. R. V. Z. Jonathan R. McDonough, “Intensified carbon capture using adsorption: Heat transfer challenges and potential solutions,” 2018.

[8] A. Kalam, “Power to X & Energy of the Future,” Energy Central, 2020.

[9] J. L. F. M. A. M. K. F. G. S. B. R. R. Manuel Gotz, “Renewable Power-to-Gas: A technological and economic review,” 2015.

[10] H. L. J. Y. L. L. Z. Y. X. Y. Qie Sun, “Selection of appropriate biogas upgrading technology-a review of biogas cleaning, upgrading and utilisation,” 2015.

[11] M. C. J.-M. J. Cristina Calderón, “Bioenergy Europe statistical report,” 2020.

[12] A. P. a. M. G. Luca Benedetti, “Biogas and Biomethane in Italy,” 2021.

[13] M. Torrijos, “State of Development of Biogas Production in Europe,” 2016.

[14] W. I. M. S. A. W. Piotr Sulewski, “Development of the Biomethane Market in Europe,” 2023.

[15] K. A. A. E. A. d. S. C. E. B. a. C. A. G. Rafael Luan Sehn Canevesi, “Pressure swing adsorption for biogas upgrading with carbon molecular sieve,” 2018.

[16] T. Kim, “Dynamic Modeling and Simulation of Pressure Swing Adsorption,” 2023.

[17] C. W. Skarstrom, “Method and Apparatus for Fractionating Gaseous Mixtures by,” 1960.

[18] S. M. Gawande, “Adsorption and its isotherm,” 2017.

[19] Y. L. a. Y. Y. Kevin R. Wood, “Design, Simulation, and Optimization of Adsorptive and Chromatographic Separations,” 2018.

[20] C. R. Girish, “VARIOUS ISOTHERM MODELS FOR MULTICOMPONENT ADSORPTION: A REVIEW,” *International Journal of Civil Engineering and Technology,* 2017.

[21] J. K. S. Taehun Kim, “Dynamic Modeling and Simulation of Pressure Swing Adsorption Processes using toPsail,” *Georgia Institute of Technology , Department of Chemical & Biomolecular Engineering,* 2023.

[22] S.Ergun, Fluid Flow Through Packed Columns, Chemichal Engineering Progress, 1999.

[23] A. P. M. Haripriya Naidu, “Linear driving force analysis of adsorption dynamics in fixed-bed adsrobers,” *Separation and Purification Technology,* 2021.

[24] F. H. T. Peter J.E. Harlick, “An experimental adsorbent screening study for CO2 removal from N2,” 2004.

[25] M. C. F. M. Jerome MErel, “Experimental Investigation on CO2 Post−Combustion Capture by Indirect Thermal Swing Adsorption Using 13X and 5A Zeolites,” 2007.

[26] D. L. J. A. T. M. Kenji Sumida, “Carbon dioxide capture in Metal-Organic Frameworks,” 2011.

[27] M.-S. S. E. P. J. A. Ranjani V.Siriwardane, “Adsorption of CO2 on Molecular Sieves and Activated Carbon,” 2001.

[28] C. P. T. E. D. B. Frederik Berg, “Temperature Swing Adsorption in Natural Gas Processing: A concise Overview,” 2019.

[29] Y. S. B. L. D. Z. Z. T. G. L. B. F. Nan Jianga, “CO2 capture from dry flue gas by means of VPSA, TSA and TVSA,” *Journal of CO2 Utilization,* 2019.

[30] J. H. D. K. Y. W. J.D. Holladay, “Catalysis Today,” 2008.

[31] G. B. a. G. C. Linda Barelli, “Airflow Management in Solid Oxide Electrolyzer (SOE) Operation: Performance Analysis,” 2017.

[32] R. C. Leonardo Vidas, “Recent Developments on Hydrogen Production Technologies: State-of-the-Art Review with a Focus on Green-Electrolysis,” 2021.

[33] J. D. K. Y. J.D. Holladay, “An overview of hydrogen production technologies,” 2009.

[34] I. Ulleberg, “Modeling of advanced alkaline electrolyzers: a system simulation approach,” *International Journal of Hydrogen Energy,* 2003.

[35] L. M. G. a. P. S. Alfredo Ursua, “Hydrogen Production From Water Electrolysis: Current status e future trends,” 2011.

[36] I. Ulleberg, “Modeling of advanced alkaline electrolyzers: a system simulation approach,” 2003.

[37] J. R. O. A. d. L.-C. Ernesto Amores, “Development of an operation strategy for hydrogen production using solar PV energy based on fluid dynamic aspects,” 2017.

[38] E. A. D. A. L. R. C. C.-. J. Monica Sanchez, “Aspen Plus model of an alkaline electrolysis system for hydrogen production,” 2019.

[39] E. A. L. R. C. C.-J. Monica Sanchez, “Semi-empirical model and experimental validation for the performance evaluation of a 15 kWalkaline water electrolyzer,” 2018.

[40] X. Z. ,. Y. J. ,. G. S. J. S. S. Z. K. W. Min Liu, “Mathematical Modeling and Experimental Validation for a 50 kW Alkaline Water Electrolyzer,” 2024.

[41] A. J. N. H. M. H. I. Hussaina, “Recent advances in catalytic systems for CO2 conversion to substitute natural gas (SNG): Perspective and challenges,” *Journal of Energy Chemistry,* 2021.

[42] J. M. P. a. N. U. A. J. H. Jensen, “From coal to green energy,” 2011.

[43] “Review on methanation – From fundamentals to current projects,” 2016.

[44] J. Y. a. C.-H. Lee, “Separation of Hydrogen Mixtures by a Two-Bed Pressure Swing Adsorption Process Using Zeolite 5A,” 1997.

[45] R. D. H. J. L. K. N. J. Brasington, E. G. Lewis, L. L. Pinkerton, M. J. Turner, E. Varghese and M. Woods, “Cost and Performance Baseline for Fossil Energy Plants Volume 2: Coal to Synthetic Natural Gas and Ammonia,” 2011.

[46] S. R. GAS, “SPECIFICA TECNICA SULLE CARATTERISTICHE CHIMICO-FISICHE E SULLA PRESENZA DI ALTRI COMPONENTI NEL GAS NATURALE E NEL BIOMETANO”.

[47] D. M. G. M. O. K. A. M. P. Marocco, “A study of the techno-economic feasibility of H2-based energy storage systems in remote areas,” 2020.

[48] ENEA, “THE POTENTIAL OF POWER-TO-GAS,” 2016.

[49] H. B. D. C. R. R. T. Andreas Zauner, “Innovative large-scale energy storage technologies and Power-to-Gas concepts after optimization,” 2019.

[50] B. World, “Biogas Upgrading to Biomethane: Discover BiogasWorld’s Clients and their Technology”.

[51] R. R. B. a. Y. Y. Alexandra M Oliveira, “A green hydrogen economy for a renewable,” 2021.

[52] M. A. A. A. Y. A. H. Hamid Zentou, “Advancements and Challenges in Adsorption-Based Carbon Capture Technology: From Fundamentals to Deployment,” *T H E C H E M I C A L R E C O R D,* 2025.

[53] R. M..

[54] C. A. P. L. J. Y. A. E. Zhen Liu, “Multi-bed Vacuum Pressure Swing Adsorption for carbon dioxide capture from flue gas,” 2011.

[55] V. A. ,. G. J. W. E. Spyridon Achinas, “A Technological Overview of Biogas Production from Biowaste,” 2017.

[56] A. Godula-Jopek, Hydrogen Production by electrolysis, 2015.

[57] H. Topsoe, “From solid fuels to substitute natural gas (SNG) using TREMP™,” 2009.

[58] R. O. D. M. W. J. D. Shane McDonagh, “Modelling of a power-to-gas system to predict the levelised cost of energy of an advanced renewable gaseous transport fuel,” 2018.